

Atomic Force Microscopy of Biopolymers on Graphite Surfaces

E. V. Dubrovin^{a,b*} and D. V. Klinov^{b,c}

^a Faculty of Physics, Moscow State University, Moscow, 119991 Russia

^b Federal Research and Clinical Center of Physical-Chemical Medicine,
Federal Medical Biological Agency, Moscow, 119435 Russia

^c Sirius University of Science and Technology, Sochi, 354340 Russia

*e-mail: dubrovin@polly.phys.msu.ru

Received March 15, 2021; revised May 27, 2021; accepted July 29, 2021

Abstract—The main peculiarities of the interaction of DNA and protein molecules with graphite are considered. The results of atomic force microscopy study of the adsorption of DNA and proteins on the surface of highly oriented pyrolytic graphite are analyzed. These data are compared with the results of molecular dynamics simulation and optical studies. The dehybridization of DNA and the denaturation of many proteins on the graphite surface which are predominantly associated with π – π -stacking interaction (for DNA and proteins) and van der Waals and hydrophobic interactions (for proteins) are discussed. It is shown that the surface of highly oriented pyrolytic graphite is strongly liable to random environmental contaminations that considerably change the properties of the surface and, therefore, influence the kinetics of adsorption of biopolymer molecules and their conformation on the surface. Considerable attention is given to analysis of the interaction of biopolymers with the surface of highly oriented pyrolytic graphite modified with monolayers of organic molecules.

DOI: 10.1134/S0965545X2106002X

INTRODUCTION

The Use of AFM for the Study (of Adsorption) of Biopolymers

Soon after its invention in 1986 [1], atomic force microscopy became a widely used tool for studying biopolymers, in particular, DNA and proteins, and various biopolymer complexes and structures (the first reviews on this subject had been published already in a few years [2, 3]). Owing to its high spatial resolution attaining for soft biological objects 0.5 nm in the lateral direction and 0.1 nm in the vertical direction [4], AFM allows visualization of single biopolymer molecules and molecular complexes and revealing of their conformational features on the nanoscale.

Even though the resolution of modern electron (or helium ion) microscopes is frequently higher than the resolution of AFM, a crucial part of information acquired by AFM remains unique and supplements the results of other research techniques [5, 6]. This is associated with the fact that AFM can operate under conditions inapplicable to electron (or helium ion) microscopy and can determine characteristics of the sample that are hardly obtainable by other high-resolution microscopy techniques. For example, AFM makes it possible to operate in air and aqueous media (which are generally more natural for biological molecules than vacuum) and to use electron opaque substrates (e.g., highly oriented pyrolytic graphite,

HOPG), does not require metallization or preparation of microcross sections of the sample, and, finally, enables one to investigate dynamic processes in the real-time mode. Despite the intense development of low-vacuum transmission electron microscopy (TEM), which allows one to operate in water vapor or aqueous solutions, it cannot replace AFM. TEM studies require complex preparation of the sample and selection of operating parameters, and the resolution of this technique, as applied to biological objects, markedly ranks below the resolution of high-vacuum microscopy [7, 8]. Furthermore, modern atomic force microscopes provide broad opportunities for mapping mechanical, optical, electrical, and chemical properties of the test sample on the nanoscale.

The adsorption of a biopolymer on a solid surface is a necessary condition for its AFM imaging. In addition, the adsorption of biopolymers itself is of great fundamental and applied importance. For example, the adsorption of plasma proteins on the surface of antigen happens already from the first seconds after it enters the body, and the biocompatibility of a material is largely determined by the adsorption features of proteins of the contacting biological liquid on it [9–11]. In addition, the adsorption of biopolymers on the surface is utilized for designing various biotechnological devices, for example, biosensors and adsorption chromatographs [12]. Finally, along with AFM, there are other techniques for surface studies which imply

adsorption of the test object on the surface (e.g., quartz microbalance, ellipsometry, surface plasmon resonance) but lack (sub)nanometer spatial resolution. Therefore, AFM capable of elucidating conformational, morphological, kinetic, mechanical, and other features of adsorbed molecules is an important tool for studying the adsorption of biopolymers which is demanded in both fundamental and applied research.

The AFM analysis of biopolymers is used to solve challenges in various research areas, including biophysics, polymer physics, molecular biology, biotechnology, and medicine. In particular, AFM made a considerable contribution to the investigation of conformations of DNA and proteins and the structure of protein-protein and nucleoprotein complexes [13–16], a number of molecular biological processes (translation [17], transcription [18], and replication [19]), protein amyloid aggregation [20], and surface diffusion of biopolymers [21]. Accordingly, using theoretical ideas about the structure and properties of polymers, a special methodology was developed for the analysis of conformations of biopolymers from the AFM data.

The tapping mode of AFM operation is used most frequently in the study of biopolymers [22]. In this mode, a cantilever is driven to oscillate with a frequency close to the resonance one, and interaction with the surface entails reduction in its oscillation amplitude. This value serves as a feedback for imaging. In the tapping mode, the cantilever acts on the sample with forces on the order of 10 nN and makes it possible to minimize the impact of capillary forces worsening the resolution of a microscope [23]. In the past decade, the tapping mode has gradually been displaced by the PeakForce tapping mode or similar modes called the hybrid mode, jumping mode, or pulsed force mode. These modes are based on measuring the force curve (dependence of the force of interaction of a cantilever with the surface on the vertical displacement between the sample and the cantilever) at each point of the image raster. The PeakForce mode can minimize the force of interaction of the cantilever with the sample to values on the order of several tens of piconewtons [23].

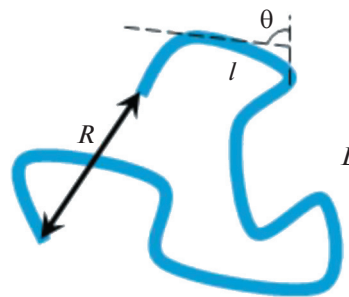
Methodology of Analysis of Polymer Conformations from AFM Images

If resolution of the AFM image enables one to trace the contour of adsorbed polymer molecules (it is often realized for DNA molecules), then it becomes possible to analyze polymer conformations using the statistical analysis of the contours of polymer molecules. For this purpose, the so-called scaling exponent ν is often calculated from the ratio

$$\langle R^2 \rangle = \text{const} \times L^{2\nu}, \quad (1)$$

where $\langle R^2 \rangle$ is the root mean square end-to-end distance of a polymer molecule and L is its contour length; the values of R and L are determined directly from the AFM images of polymer molecules [24]. The value of ν , along with analysis of the presence of contour self-intersections of a polymer, makes it possible to assign a certain conformation to it. For example, $\nu = 1$ corresponds to the rigid rod conformation (a molecule is linearly extended, self-intersections are excluded), $\nu = 0.75$ corresponds to the self-avoiding random walk conformation in the absence of self-intersections, $\nu \approx 0.59$ corresponds to the two-dimensional projection of the three-dimensional coil (kinetic trapping by the surface) in the presence of self-intersections, and $\nu = 0.5$ corresponds to the compact globule conformation in the absence of self-intersections [6, 25, 26].

If a polymer molecule can be treated as a uniform elastic cylinder (this case is usually realized for DNA [27]), conformations are described by the wormlike chain (or persistence) model.



Within the framework of this model the distribution of angle θ between tangents drawn at two points of the polymer contour separated by the contour length l is Gaussian [28]:

$$N(\theta(l))_{2D} = \sqrt{\frac{P}{2\pi l}} e^{-\frac{P\theta^2}{2l}}, \quad (2)$$

where P is the persistence length, which is a measure of flexibility of a polymer molecule, and index 2D implies that the formula describes the two-dimensional case of the persistence model.

In practice, the persistence length is assessed from one of the three ratios derived from formula (2):

$$\langle \theta^2 \rangle = l/P; \quad (3)$$

$$\langle \cos(\theta) \rangle = e^{-\frac{l}{2P}}; \quad (4)$$

$$\langle R^2 \rangle_{2D} = 4Pl \left[1 - \frac{2P \left(1 - e^{-\frac{l}{2P}} \right)}{l} \right]. \quad (5)$$

Note that ratios (3)–(5) do not take into account repulsion between various polymer units (the excluded

volume effect). This approximation is valid when the contour length of a polymer is not above $20P$ [27].

For the justified application of the persistence length parameter, the system under study should match the wormlike chain model [28]. The value of P is often estimated through one of formulas (3)–(5) without analysis of the applicability of the wormlike chain model to the system. In this case, it makes sense to talk about the “effective” or “measured” persistence length.

In the case of polymer adsorption according to the scenario of kinetic trapping by the surface, P can be determined using the following ratio between the root mean square distance $\langle R^2 \rangle$ and contour length of the polymer l [27]:

$$\langle R^2 \rangle_{\text{project}} = \frac{4}{3} Pl \left(1 - \frac{P \left(1 - e^{-\frac{l}{P}} \right)}{l} \right). \quad (6)$$

Substrates for the AFM Study of Biopolymers

A high level of smoothness of the substrate surface is a vital factor in the AFM study of biopolymers because as a minimum one of their sizes is usually in the nanometer range (e.g., the diameter of B-DNA is 2 nm and the diameter of a molecule of a large globular protein, ferritin, is 12 nm). Owing to the presence of extended (hundreds of square microns) regions of the surface with atomic smoothness and a relatively low price, mica is the most popular substrate for the AFM of biopolymers.

Mica belongs to the class of layered aluminosilicate crystals characterized by a negative charge of aluminosilicate layers compensated by univalent cations (e.g., K^+ in the muscovite mica) arranged between layers [29]. When the mica surface is immersed in water, the dissociation of cations occurs, which leads to appearance of the negative surface charge (-0.0025 C/m^2 at neutral pH [30]). This in turn hampers the adsorption of like-charged biopolymers (e.g., DNA). Therefore, for the adsorption of such molecules, the surface of mica is modified, for example, with divalent cations [31] or aminosilanes [13].

When mica is cleaved in air, the reaction between atmospheric CO_2 , water, and mica results in the formation of potassium carbonate (K_2CO_3) on its surface (surface concentration, $\approx 1 \text{ molecule/nm}^2$), which crystallizes at a low humidity [32]. Formation of the salt on the mica surface may trigger effects undesirable for the AFM of biopolymers, such as high and uncontrolled ionic strength in aqueous solution near the substrate surface [33, 34] and an underestimated height of the adsorbed molecule immersed in the salt film.

An alternative to mica as a substrate for AFM studies is HOPG. The surface of HOPG is a hexagonally packed lattice composed of carbon atoms in the sp^2 hybridization which contains extended regions of the atomically smooth surface. However, as opposed to the mica surface, the surface of HOPG is electrically neutral and chemically inert (except step edges) and has a high electrical conductivity. The peculiar properties of HOPG and its derivatives, such as fullerenes, carbon nanotubes (CNTs), and graphene, make them attractive materials for designing biosensors, catalysts, and molecular electronic devices [35–39]. In addition, pyrolytic graphite is utilized as a material for implants [9, 40, 41], and graphite structures modified with biomolecules show great promise as biocompatible and water-soluble materials for biomedical applications, including drug delivery [42, 43]. Thus, understanding of the peculiarities of interaction of biopolymer molecules with graphite surfaces, on one hand, is of a great methodological value for the development of AFM of biopolymers on graphite and, on the other hand, is of independent scientific and applied interest.

The Scope of Analyzed Results

Despite a large quantity of AFM studies of biopolymers on the graphite surface, there is a certain inconsistency in the data on the conformation of DNA and proteins on graphite surfaces. Analytical reviews on this subject are unavailable. The goals of this review are analysis, systematization, and generalization of scientific achievements directly related to the AFM probing of biopolymers (primarily DNA and proteins) on graphite surfaces.

Among them are the detection and visualization of the HOPG surface-induced denaturation of many proteins and a strong liability of the HOPG surface to random environmental contaminations that considerably change the surface properties of HOPG and, therefore, influence the kinetics of adsorption of biopolymer molecules and their conformation on the surface. Particular attention will be focused on the use of HOPG surfaces modified with various organic compounds that make it possible to change the properties of the graphite surface, imparting a certain charge and degree of hydrophilicity/hydrophobicity to it and creating a certain nanorelief of the surface.

Modified HOPG surfaces are of great interest as substrates in the AFM of biopolymers, because in some cases they considerably increase the informativeness of the structural analysis of single biopolymer molecules in comparison to other surfaces. Moreover, the modified HOPG is important for tailoring biocompatible materials. According to analysis of the published data, prospects for using HOPG as a substrate for fundamental AFM studies and biomedical and biotechnological applications are formulated.

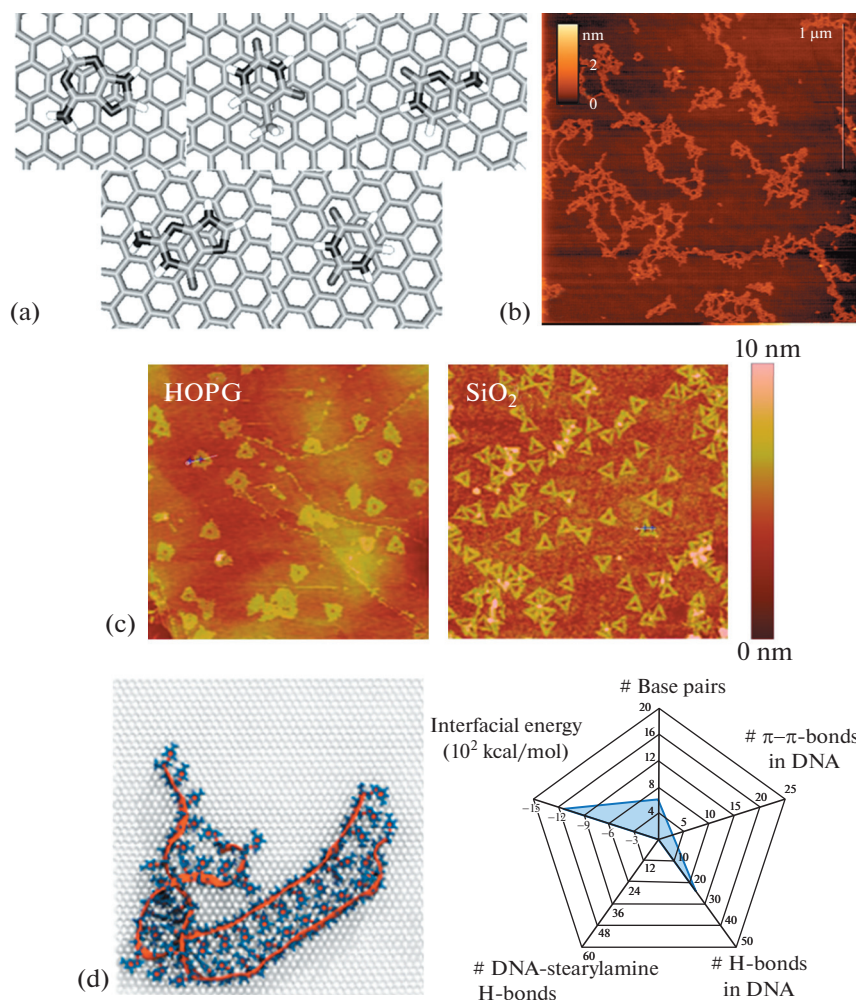


Fig. 1. (a) Structures of DNA bases (adenine, thymine, cytosine, guanine, and uracil) on C₉₆H₂₄ optimized using the density functional theory with allowance made for the dispersion correction. Republished with permission of Royal Society of Chemistry, from [50]; permission conveyed through Copyright Clearance Center, Inc. (b) AFM image ($2 \times 2 \mu\text{m}^2$) of linearized plasmid DNA (2000 base pairs) molecules adsorbed on the freshly cleaved HOPG surface. Reprinted with permission from [126]. Copyright (2014) American Chemical Society. (c) AFM images ($3 \times 3 \mu\text{m}^2$) of triangular DNA origami nanostructures on the surface of HOPG (on the left) and SiO₂ (on the right) (images were obtained in the tapping mode in air). Reprinted with permission from [54]. Copyright (2017) American Chemical Society. (d) All-atom molecular model of the fragment of a DNA molecule ((GC)₂₅) adsorbed on the graphene surface is on the left; the diagram of correlation between the average number of base pairs, internal π - π bonds, internal hydrogen bonds, DNA-stearylamine hydrogen bonds (for comparison with the system shown in Fig. 4g), and the interfacial energy of the DNA surface corresponding to this model is on the right. Reprinted with permission from [57]. Copyright (2020) American Chemical Society. Color drawing can be viewed in the electronic version.

INTERACTION OF BIOPOLYMERS WITH A FRESHLY CLEAVED HOPG SURFACE

DNA

DNA is a long chain of alternating nucleotides (adenine, cytosine, guanine, thymine) arranged on the deoxyribose framework and linked by phosphodiester bonds. Single-stranded DNA molecules are adsorbed well on the surface of graphite materials, such as CNTs [44], graphene [38, 45], and HOPG [46, 47]. Model experiments, theoretical calculations, and molecular simulation showed that the major

mechanism behind the noncovalent immobilization of DNA on graphite surfaces is π - π stacking between single DNA bases and aromatic structures of the graphite surface which fit each other well (Fig. 1a) [48–50]. The strength of interaction of bases with the graphite surface changes in the following sequence: guanine > adenine > thymine > cytosine [46, 51, 52]. It was shown that energy of the stacking interaction of nucleotide bases with the graphite surface (–20 to –25 kcal/mol) is comparable with the energy of hydrogen bonds formed by a Watson–Crick nucleotide base pair [50].

The adsorption of double-stranded DNA on graphite surfaces is generally weaker than that of the single-stranded one [53–56]. Double-stranded DNA molecules are adsorbed on the freshly cleaved HOPG surface as branched and interlaced structures that do not make it possible to distinguish single biopolymer molecules (Fig. 1b). The adsorption of triangular DNA origami nanostructures on the HOPG surface is accompanied by a marked increase in their thickness compared with the thickness of structures adsorbed on the SiO₂ surface (Fig. 1c) [54].

The specific nature of double-stranded DNA adsorption on the graphite surface can be explained by the peculiarities of interaction of nucleotide bases with graphite. During the adsorption of double-stranded DNA on the graphite surface DNA can experience deformation or partial dehybridization (unwinding of the double helix) which triggers the emergence of nucleotide bases at the graphite surface and the formation of π – π stacking [54, 55]. This leads to the disruption of integrity and loss of rigidity of the DNA double helix adsorbed on graphite and to an increase in the thickness of DNA origami nanostructures. The loss of stability of the double-stranded DNA adsorbed on the graphite surface was convincingly proved by all-atom molecular simulation which unveiled the unwinding of the DNA double helix and a reduction in the number of both hydrogen bonds and π – π bonds in a DNA molecule (Fig. 1d) [57]. Thus, the bare HOPG surface is inapplicable for use in the AFM studies of DNA and DNA–protein complexes. For this purpose, the HOPG surface is modified with organic molecules (section Adsorption of Biopolymers on the Modified HOPG Surface).

Proteins

Proteins are characterized by the hierarchical structure including primary (the sequence of amino acid residues), secondary (α -helices and β -structures), tertiary, and quaternary structures. During the adsorption of protein on a substrate, the environment of a protein molecule from the side of its contact with the surface changes: water molecules are “replaced” by the surface. This may cause a change in the balance of forces (van der Waals, hydrophobic, electrostatic, hydrogen bonds) between parts of a protein molecule and entail conformational rearrangements, for example, partial or full denaturation of the protein molecule [58–60]. Therefore, the conformation of adsorbed proteins, generally speaking, differs from the native conformation of a protein in solution. The conformational changes of the protein upon adsorption are of utmost importance in biomedicine and biotechnology; in particular, they can activate certain biological processes (e.g., launch the complement system [61]), reduce the catalytic activity of enzymes adsorbed on the solid surface [62], and increase the toxicity of protein-modified nanoparticles [63].

Proteins were conditionally classified into “soft” and “hard” depending on their liability to conformational changes [60, 64]. The examples of “soft” proteins are myoglobin, fibrinogen, casein, and immunoglobulins; they are characterized by a less stable tertiary structure, a stronger deformation, and unfolding on the surface. The examples of “hard” proteins are lysozyme, cytochrome C, and superoxide dismutase; these proteins typically do not experience considerable conformational changes during adsorption on the surface.

The properties of the surface largely determine the degree and character of conformational changes of a protein adsorbing on it. Changes in the secondary structure of proteins are traditionally detected using such techniques as circular dichroism [65, 66], attenuated total internal reflection spectroscopy [67, 68], and neutron reflectometry [69]. These techniques are based on the analysis of a section of the surface containing ensembles of a large number of molecules. For example, it was shown that hydrophobic surfaces as a rule facilitate a stronger unfolding of globular proteins than hydrophilic surfaces [70]. Traditional techniques do not provide information about conformational changes of single protein molecules. AFM data supplement the results of optical techniques on the conformational, kinetic, and mechanical properties of adsorbed proteins at the level of single molecules with (sub)nanometer spatial resolution.

The study of adsorption of proteins on graphite surfaces primarily addresses plasma proteins, such as fibrinogen, IgG antibodies, and serum albumins. Gaining insight into their interaction with graphite is especially important for biomedicine and biotechnology; therefore, let us discuss them in more detail.

Fibrinogen is a glycoprotein with $M = 34 \times 10^4$ which is made up of three pairs of polypeptide chains ($A\alpha$, $B\beta$, and γ)₂ arranged into a trinodular structure with one central and two external globular regions linked by helical sections. A fibrinogen molecule also contains the unstructured C terminus of $A\alpha$ chains with a length of 390 amino acid residues, which is called the α C region. All six chains are held together by 29 disulfide bonds [71].

The AFM studies of fibrinogen on the HOPG surface in a phosphate buffered saline led to contradictory data on the conformation and dynamics of adsorption of protein molecules. The authors of [72] report that, immediately after deposition of fibrinogen (concentration, 50 μ g/mL), a network monolayer with a height of 3–4 nm is formed whose area increases, and within \sim 225 s it transforms into a solid monolayer. Thirty minutes after deposition of a fibrinogen solution on the HOPG surface, globular aggregates with a height of 8–60 nm emerge, which are probably formed on the initial fibrinogen layer [72, 73]. In [74], a network adsorbate with a height of about 1 nm appeared on the HOPG surface already 1 min

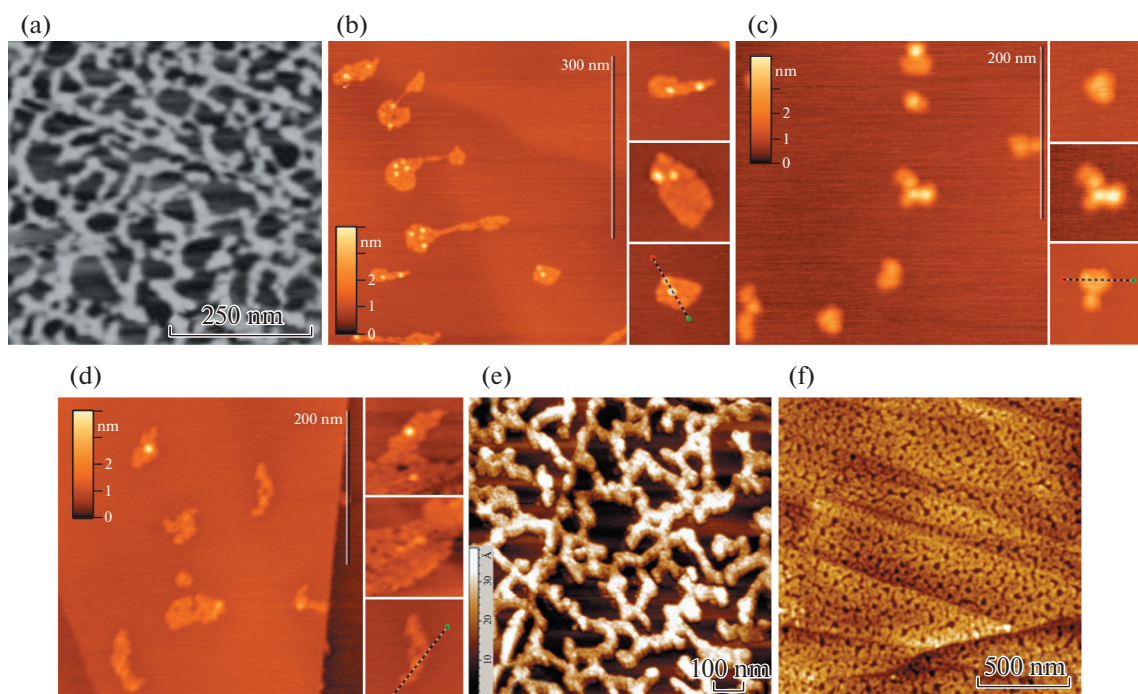


Fig. 2. (a) Structures formed 60 min after deposition of fibrinogen (concentration, 2.5 $\mu\text{g}/\text{mL}$) on the HOPG surface (height difference, 10 nm). Reprinted with permission from [77]. Copyright (2005) Wiley Periodicals Inc. (b–d) Molecules of (b) fibrinogen, (c) IgG, and (d) human serum albumin (10–50 $\mu\text{g}/\text{mL}$) adsorbed on the HOPG surface for 10 s. Reprinted from [79]. Copyright (2016), with permission from Elsevier. (e) Structures formed 1 min after deposition of human serum albumin (concentration, 10 $\mu\text{g}/\text{mL}$) on the HOPG surface. Reprinted with permission from [86]. Copyright (2015) Wiley Periodicals Inc. (f) AFM image of the HOPG surface incubated in solution of dodecamer peptide GAMHLPWHMGTL. Reprinted with permission from [91]. Copyright (2012) American Chemical Society. The images were obtained in air.

after deposition of fibrinogen (7 $\mu\text{g}/\text{mL}$). In the cited studies, no adsorption of single molecules on the graphite surface was observed. According to the authors, this observation can be attributed to a stronger lateral interaction between protein molecules than with the HOPG surface [72] or the denaturation of protein during adsorption [74]. At the same, the authors of [75] observed the adsorption of single fibrinogen molecules (0.5–1 $\mu\text{g}/\text{mL}$) on the HOPG surface, which was confirmed by the typical trinodular structure of molecules; the height of their globular parts decreased from ~ 2 to ~ 1 nm for 130 min.

In several AFM studies, the adsorption of fibrinogen on the HOPG or graphene surface was carried out in air after drying the sample. K.L. Marchin and C.L. Berrie described the tendency of fibrinogen to form clusters (aggregates) with a height of ~ 1 nm on the HOPG surface, although fibrinogen was also adsorbed on the surface as single extended molecules with a height of ~ 1 nm and a length of ~ 63 nm (0.05–10 $\mu\text{g}/\text{mL}$; adsorption time, 10 min) [76]. According to these authors, these sizes can be explained by the spreading of a fibrinogen molecule on the HOPG surface induced by the unfolded configuration of its αC regions. The formation of similar fibrinogen clusters on the HOPG surface was reported by Gettens et al.

[77] at a low fibrinogen concentration (0.01–1 $\mu\text{g}/\text{mL}$) and/or a short time after deposition of the sample (5–15 min). As the concentration or adsorption time was increased, network protein layers developed (Fig. 2a). In both papers, the adsorption of fibrinogen along step edges prevailed. Extended molecules and fibrinogen clusters were also observed by R. Ohta et al., who interpreted the underestimated height (~ 1.5 nm) and overestimated lateral sizes (compared with the known crystallographic data) by the denaturation of fibrinogen upon adsorption on the HOPG surface [78]. N.A. Barinov et al. showed that, upon deposition of fibrinogen (10–50 $\mu\text{g}/\text{mL}$) on the freshly cleaved HOPG surface for 10 s, single partially denatured fibrinogen molecules are present which contain external globules with a height of 2.5 ± 0.3 nm immersed in the adsorbate layer with a height of 0.5–1.0 nm (Fig. 2b) [79].

Thus, in most AFM studies on the adsorption of fibrinogen on the HOPG surface, the formation of protein clusters and/or network layers is observed, as well as the predominant adsorption of single molecules and clusters along graphite step edges. Different authors report different heights of the emerging structures (1–4 nm). There is also a certain contradiction in estimating the reversibility of fibrinogen adsorption on

the HOPG surface: according to [77], the adsorption of fibrinogen on the HOPG surface is reversible, whereas the authors of [72] describe a strong adhesion of fibrinogen on the HOPG surface and even stability of network fibrinogen structures to washing by detergent (3% sodium dodecyl sulfate).

Antibodies IgG belong to the family of highly conserved glycoproteins consisting of two identical pairs of polypeptide chains: light ($M = 25 \times 10^3$) and heavy ($M = 50 \times 10^3$) linked together by disulfide bonds. Polypeptide chains form a Y-shaped molecule containing two Fab fragments (containing antigen-binding region) and one terminal Fc fragment [80].

Cullen and Lowe [81], who carried out the AFM study in the phosphate saline buffer, showed that IgG molecules (50 $\mu\text{g}/\text{mL}$) are adsorbed on the HOPG surface in the form of sheets containing 300–500 molecules. In the course of time, the area of sheets increases and they turn into a monolayer with 2–3 nm grooves. These data made it possible to propose the native structure of the adsorbed protein. J.G. Vilhena et al. also did not uncover signs of denaturation of IgG molecules adsorbed on the graphene surface. Nevertheless, they observed the adsorption of single IgG molecules on the graphene surface and unraveled several orientations of adsorbed IgG molecules differing in height and morphology, including the flat orientation and three types of the vertical orientation. Given this, a noticeable proportion of orientations were characterized by Fab fragments reversed away from the surface, which should imply that biofunctionality of the adsorbed protein is preserved [82]. However, a recent AFM probing in air demonstrated that, 10 s after deposition, IgG molecules spread on the freshly cleaved HOPG surface and their height is decreased to 1.1 ± 0.3 nm, which suggests a strong denaturation of adsorbed antibodies (Fig. 2c) [79].

Serum albumin is the basic protein of mammal blood plasma having a molecular weight of 67×10^3 . It consists of a single polypeptide chain crosslinked by 17 disulfide bonds. Serum albumins of various mammals are highly homologous in structure and are composed primarily of α -helices arranged into three similar domains forming the heart-shaped structure of a molecule [83].

The AFM study of bovine serum albumin adsorption on the HOPG surface in the phosphate saline buffer revealed that, 30 min after protein deposition, graphite globular aggregates with a height of 6–13 nm (at a protein concentration of 50 $\mu\text{g}/\text{mL}$) or segregated domains with a height of 1.7 ± 0.3 nm (at a protein concentration of 10 $\mu\text{g}/\text{mL}$) appear on the basal graphite plane [73]. This short height of domains indicates that bovine serum albumin undergoes denaturation on the HOPG surface. A strong denaturation of single human serum albumin molecules was observed already several seconds after deposition of protein (10 $\mu\text{g}/\text{mL}$) on the freshly cleaved HOPG surface [79]

(Fig. 2d). Bovine serum albumin single molecules electrospayed on the HOPG surface were adsorbed both on the HOPG basal surface and on step edges; on step edges, adsorption was usually stronger, which was probably associated with the presence of a charge on them [84]. The character of adsorption and the sizes of a molecule made it possible to assume the denaturation of protein; however, it could have occurred during deposition.

In another AFM study [85], human serum albumin was adsorbed on the HOPG surface from solution of a low concentration (1 $\mu\text{g}/\text{mL}$) in the form of single native-like molecules (i.e., molecules having the shape close to the shape of native molecules) with a height of ~ 3 nm, whereas upon deposition from solution of a higher concentration (100 $\mu\text{g}/\text{mL}$) human serum albumin formed the network structure. The authors of [86] also observed native-like human serum albumin molecules with a height of 1.91 ± 0.22 nm on graphite upon adsorption from solution of a low concentration (1 $\mu\text{g}/\text{mL}$; the incubation time, 72 min) and detected the formation of network films with a height of 2.2 ± 0.3 nm as the protein concentration was increased to 10 $\mu\text{g}/\text{mL}$ (Fig. 2e).

The AFM studies of the adsorption of glucoxidase [81], cytochrome C [87], fibronectin [85], and laccase [88] on the HOPG surface revealed that these proteins formed network films with height from 0.5 to 3 nm, which indicated a stronger interaction of protein molecules with each other than with the graphite surface. Molecules of platelet membrane receptor $\alpha\text{IIb}\beta_3$ and membrane arabinogalactan (AGP) and octapeptide NAP were adsorbed on the HOPG surface in the form of globules or their aggregates and did not form network structures [89].

Thus, the character of adsorption of proteins on the graphite surface strongly depends on the protein nature, its initial concentration, and adsorption time. The adsorption of single molecules is usually observed at relatively low concentrations and incubation times. As the indicated parameters are increased, the molecules aggregate on the surface and form conglomerates, branched networks, and layers. In many cases, proteins undergo unfolding on the graphite surface.

The conformational and functional changes of proteins adsorbed on graphite surfaces were investigated using additional techniques. For example, circular dichroism measurements showed that, upon the adsorption of fibrinogen, gamma-globulin, and bovine serum albumin on the CNT surface, the fraction of α -helices declines appreciably, while the fraction of β -structures grows; for fibrinogen and gamma-globulin these changes are irreversible, while for bovine serum albumin they are partially reversible [90]. Attenuated total internal reflection IR spectroscopy studies uncovered a blue shift of amide regions of a 12-unit graphene-binding peptide adsorbed on the HOPG surface, which was interpreted as distortion of

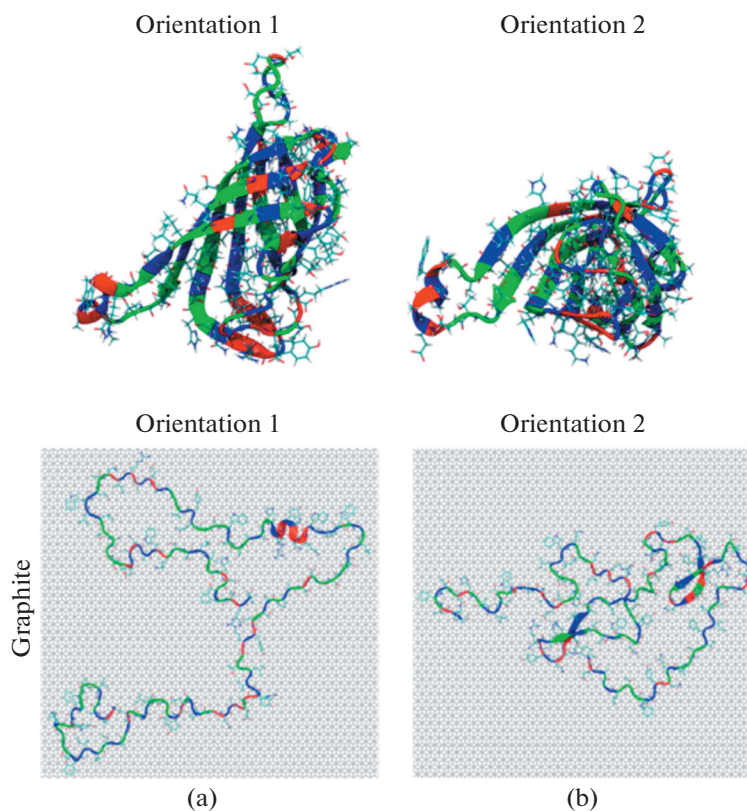


Fig. 3. Results of the molecular simulation of streptavidin adsorption on the graphite surface: (a) primary orientations of the protein molecule and (b) conformation of a streptavidin molecule after 40 ns for each primary orientation. Reprinted with permission from [102]. Copyright (2016) American Chemical Society.

the α -helical structure of the peptide owing to interaction with the surface [91]. In terms of morphology, a peptide adsorbed on the HOPG or graphene surface is a network layer with a height of about 1 nm (Fig. 2f). The authors of [92] used a quartz crystal microbalance to show that the adsorption of Concanavalin A on the graphene surface is accompanied by the loss of affinity for cell wall polysaccharides of *B. subtilis*, which can be explained by the surface-induced denaturation of protein. However, during bioconjugation of Concanavalin A to the graphene surface, it retains the ability to bind polysaccharides. In contrast, IgG lost specificity upon bioconjugation to the graphene surface [93].

Some papers concern conservation of the functionality of proteins upon their adsorption on graphite surfaces. For example, laccase molecules retain their catalytic activity upon adsorption on the HOPG surface. After covalent grafting of molecules of horseradish peroxidase (consisting mostly of α -helices) and glucosidase (composed of a mixture of α -helices and β -sheets) onto the graphene surface, the enzymatic activity of glucosidase increases, while the enzymatic activity of horseradish peroxidase decreases; this demonstrates the possible role of β -sheets in stabilization of the structure of proteins adsorbed on graphite surfaces [94].

Using sum frequency generation spectroscopy and molecular dynamic simulation, the authors of [95] demonstrated that the replacement (mutation) of two aromatic amino acid residues with alanine weakens the interaction of peptide molecules with the graphene surface and leads to a change in the flat orientation of the adsorbed peptide to the vertical one. According to these results, it was proposed that the interaction of peptides with graphene depends on competition between planar, that is, containing aromatic side groups, and hydrophilic (e.g., lysine) peptide residues.

Molecular dynamics allows a deeper insight into the character of interaction of proteins with graphite surfaces. It was shown π - π stacking plays a crucial role in the interaction of aromatic groups of tyrosine, tryptophan, and phenylalanine amino acid residues as well as histidin heterocycle with graphite surfaces [42, 90, 95, 96]. This is related to a good structural correspondence between the cyclic groups and the hexagonal graphite structure. Many CNT- and graphene-binding peptides obtained by the phage display technology were rich in aromatic and heterocyclic amino acid residues, for example, B1–B4, P1, and GrBPS [97]. Along with π - π stacking, other types of interaction, such as hydrophobic, van der Waals, and electrostatic (for charged regions of the surface, e.g., HOPG

steps), may play an important role in the interaction of proteins with graphite surfaces [94–96].

As reported in many molecular simulations of the adsorption of proteins and peptides on graphite surfaces, adsorption is accompanied by changes in the secondary structure of molecules, specifically, partial or full denaturation of a number of globular proteins (or their domains), including fibrinogen [98], human serum albumin [99–101], and others (Fig. 3) [96, 102–104]. This effect is caused by the reorientation of single domains owing to hydrophobic, van der Waals, and π - π -stacking interactions with the graphite surface. A comparison of proteins differing in size, topology, and stability demonstrated that proteins rich in β -sheets remain more stable upon adsorption on graphite than α -helical proteins [96].

EFFECT OF THE ENVIRONMENT ON THE HOPG SURFACE

It was shown several years ago that, under laboratory conditions, graphite surfaces are liable to random uncontrolled contamination by hydrocarbon impurities from the atmosphere [105]. For the HOPG surface, contamination leads to an increase in the water contact angle by $64.4^\circ \pm 2.9^\circ$ for the freshly cleaved (~ 10 s) surface to $\sim 90^\circ$ for the surface exposed in air for ~ 10 min [106, 107]. Thus, the widespread perception of HOPG and graphene as hydrophobic materials is not entirely true, and their bare surfaces are weakly hydrophilic. Adsorbed atmospheric impurities usually form films on the graphite surface [105], which commonly self-assemble into periodic lamellar structures with a lamella period of 4–5 nm [108]. In addition, it was shown that the graphite surface was contaminated by impurities evolved by a standard plastic pipette upon deposition of water on the freshly cleaved HOPG surface [109]. Here, periodic lamellar structures with a period of ~ 5 nm were also formed.

A high liability of graphite surfaces to contamination upon contact with air or liquid may be responsible for contradictory observations of the conformation and specific adsorption of proteins on the graphite. In fact, the majority of these AFM studies lack key information about the exposure time of graphite surfaces to air upon cleavage/purification before deposition of the sample, and the possible contamination of graphite from air or aqueous solution is not taken into account. The adsorption of a biopolymer on a hydrocarbon-contaminated graphite surface can be regarded as adsorption on the modified graphite surface. For example, molecular dynamic simulations revealed that the strength of adsorption of insulin on the ethane-contaminated graphite surface decreases and the protein does not denature on this surface, in contrast to the bare graphite [103]. Therefore, revisiting of a part of AFM information on biopolymers adsorbed on graphite surfaces is relevant. For example, in the case of graphite used as a substrate, it is advisable to mini-

mize the time of its contact with the environment to seconds. It should be emphasized that when the molecules of protein (fibrinogen, ferritin, human serum albumin, IgG) were deposited on the HOPG surface for 10 s after cleavage, the denaturation and spreading of molecules on the surface were observed [79].

ADSORPTION OF BIOPOLYMERS ON THE MODIFIED HOPG SURFACE

The dehybridization of DNA and the unfolding of many proteins on a bare graphite surface appreciably limit its use as a substrate for stable and well-reproducible AFM analysis of biopolymers; therefore, at the onset of the 2000s, methods of graphite surface modification began to be developed. Modification of the graphite surface changes the character of adsorption of biopolymer molecules on it and in some cases makes this surface suitable for the AFM mapping of structural, conformational, and kinetic characteristics of single biopolymer molecules.

DNA Adsorption on Plasma-Modified HOPG Surface

Glow discharging of the HOPG surface in the presence of pentylamine vapor for several seconds made it possible to modify the surface with amino groups and to maintain a low root mean square roughness of the surface (0.2–0.5 nm) [110, 111]. Thus, the modified surface allows a well-reproducible adsorption of DNA molecules in the unfolded state from aqueous or saline solution. In this case, DNA is adsorbed via electrostatic interaction between negatively charged phosphate groups of DNA and positively charged amino groups on the surface. The height of the DNA molecule on the modified HOPG surface (1.6 ± 0.3 nm), which was determined from AFM images, is higher compared with the mica surface (0.7 ± 0.1 nm). This may be associated with both the absence of saline “fringe” around a DNA molecule on the modified HOPG surface and a lower deformation of the DNA double helix than that on the mica surface. In [112], the adsorption of unfolded DNA molecules on the plasma-modified HOPG surface in the presence of water vapor occurred in the presence of univalent and divalent cations that most likely recharged the HOPG surface activated by hydroxyl groups.

Modification with Water-Insoluble Organic Compounds

The ability of organic molecules to self-assemble on the basal surface of graphite was first demonstrated for alkanes in which hydrocarbon chains are aligned along the directions of crystallographic axes of the HOPG surface [113]. Further studies showed that self-assembly on graphite surfaces (formation of the so-called nanotemplates) is a common property of many classes of organic molecules, including long-chain alkanes, alcohols, porphyrins, oligopeptides, fatty

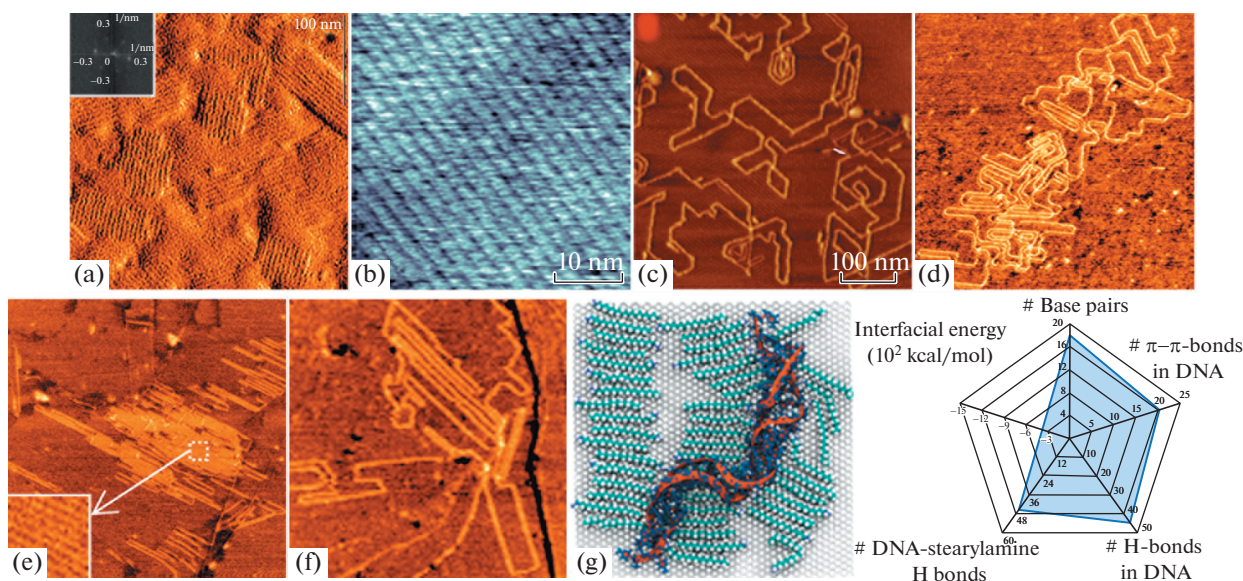


Fig. 4. (a) AFM image of the stearylamine self-assembled layer on the of HOPG surface (the Fourier transform of the image is shown on top left). Reprinted from [124]. Copyright (2010) with permission from Elsevier. (b) AFM image of the stearic acid self-assembled layer on the HOPG surface. Reprinted with permission from [119]. Copyright (2013) American Chemical Society. (c) AFM image of DNA deposited from 1 mM tris-HCl solution (pH 7.8) on the dodecylamine self-assembled layer on the HOPG surface. Reprinted with permission from [125]. Copyright (2009) American Chemical Society. (d–f) AFM images ($1 \times 1 \mu\text{m}^2$) of DNA on (d, e) stearylamine and (f) stearic acid self-assembled layer on the HOPG surface in (d) 5 mM NaCl solution, (e) 10 mM MgCl_2 solution, and (f) 10 mM NaCl solution. Reproduced from [127] under license CC BY-NC 3.0; published by the Royal Society of Chemistry. (g) All-atom molecular model of a fragment of the DNA molecule ((GC)₂₅) adsorbed on the surface of stearylamine-modified graphene is on the left; the diagram of correlation between the average number of base pairs, internal π - π bonds, internal hydrogen bonds, DNA-stearylamine hydrogen bonds, and DNA-surface interfacial energy corresponding to this mode is on the right. Reprinted with permission from [57]. Copyright (2020) American Chemical Society. (a, c–f) AFM images were obtained in the tapping mode in (a, c) air and (d–f) solution in the (a, d–f) phase and (c) height channel. (b) AFM height image was obtained in solution in the frequency modulation mode.

acids, and their derivatives (Figs. 4a, 4b) [114–120]. It was found that organic molecules self-assemble owing to van der Waals forces and hydrogen bonding between the functional groups of molecules [114, 118, 121, 122], and the fit between the length of C–C bond of a hydrocarbon chain and the graphite surface plays a significant role [116, 123]. The adsorption of DNA molecules on the HOPG surface modified with stearylamine, dodecylamine, stearic acid, and stearyl alcohol nanotemplates was investigated [47, 124–127]. To form self-assembled films, these compounds were deposited from chloroform, isopropanol, or ethanol solutions using spin coating (centrifugation) and from the vapor phase.

DNA. DNA is adsorbed on stearylamine, dodecylamine, stearic acid, and stearyl alcohol nanotemplates in the unfolded state; here, the epitaxial effect is observed; namely, the segments of adsorbed DNA molecules are elongated straightforwardly along nanotemplate lamellas directed along the third-order symmetry axes on the graphite surface (Figs. 4c–4f) [124, 126, 127]. The height of a DNA molecule on nanotemplates is generally above 1 nm, as in the case of the plasma-modified graphite surface. The contour length of DNA molecules on dodecylamine and stea-

rylamine nanotemplates is much (by 35 and 20%, respectively) higher than the theoretical length under assumption of the B form, suggesting the mechanical stretching of linearly segmented DNA molecules on these nanotemplates [124, 125].

In the case of the stearylamine self-assembled layer on the graphene surface, all-atom molecular simulation ascertained that modifier molecules enhance the conformational stability of DNA owing to the stabilization of hydrogen bonds between pair bases and stacking interaction between nucleotide pairs (Figs. 1d, 4g) [57]. Moreover, the presence of modifier molecules hinders the π - π stacking of DNA with the graphene surface and thus reduces the dehybridization of DNA adsorbed on the modified graphene surface compared with the unmodified one.

The statistical analysis of contour fluctuations of DNA molecules adsorbed on three nanotemplates on the HOPG surface, nanotemplates based on stearylamine, stearic acid, and stearyl alcohol differing only in the functional group ($-\text{NH}_2$, $-\text{COH}$, and $-\text{COOH}$), unveiled that the conformations of DNA on these surfaces are different. On surfaces of stearylamine and stearic acid nanotemplates, the adsorption

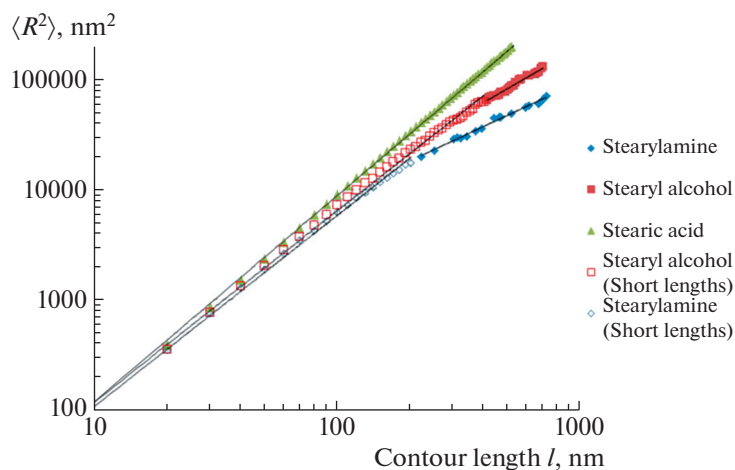


Fig. 5. Dependence of root mean square distance $\langle R^2 \rangle$ on the internal contour length l for λ -DNA adsorbed on stearylamine, stearyl alcohol, and stearic acid nanotemplates. Straight lines are linear least squares approximations of the dependences (on a double logarithmic scale). Reprinted with permission from [126]. Copyright (2014) American Chemical Society.

of DNA can be characterized differently on two scales (Fig. 5). On a short length scale (less than 200 nm for stearylamine and less than 400 nm for stearyl alcohol), the conformation of DNA is close to the rigid rod conformation ($\nu = 0.87 \pm 0.01$), which corresponds to the observed epitaxy of DNA. On a large length scale, the conformation of DNA corresponds to the two-dimensional compact globule conformation in the absence of self-crossings ($\nu = 0.52 \pm 0.02$) for stearylamine and a mixed partially relaxed conformation ($\nu = 0.66 \pm 0.02$) for stearyl alcohol [126]. The observed difference in DNA conformations on stearylamine and stearyl alcohol nanotemplates can be explained by their different interaction with DNA: with the positively charged stearylamine nanotemplate, DNA interacts primarily via electrostatic attraction, while with an almost neutral nanotemplate, stearyl alcohol, DNA interacts via van der Waals and hydrophobic interactions.

The persistence length of λ -DNA adsorbed on the stearylamine nanotemplate was estimated as 31 ± 2 nm, which is much smaller than the value obtained for DNA deposited from solution with a low ionic strength (<20 mM) on mica (~ 53 nm) [27]. This is evidence that the DNA molecule adsorbed on the stearylamine nanotemplate lost rigidity, which can be attributed to the partial neutralization of the negative charge of DNA by positively charged amino groups of the nanotemplate. It was shown that the interaction of DNA with positively charged surfaces may induce a fivefold reduction in the persistence length [128]. Another factor responsible for reduction in the persistence length is the partial denaturation of DNA on the nanotemplate, as confirmed by the presence of melting bubbles on AFM images (Fig. 4c, arrow). The partial denaturation of DNA may be driven by additional stress in a DNA molecule caused by its local

straightening upon adsorption on the nanotemplate surface [129–131].

The interaction of DNA with the stearic acid nanotemplate was weaker than that with stearylamine and stearyl alcohol nanotemplates: the conformation of DNA on this surface may be characterized by the self-avoiding random walk model in the absence of self-crossings ($\nu = 0.77 \pm 0.01$) [127], while upon drying the surface with the adsorbed DNA, the effect of molecular brushing makes itself evident which leads to the alignment of DNA molecules ($\nu = 0.93 \pm 0.01$; Fig. 5) owing to the surface tension force acting along direction of the receding liquid meniscus [126]. This behavior of DNA on the surface of stearic acid nanotemplate can be explained by a small negative charge of stearic acid hindering interaction of the surface with a like-charged DNA (this interaction remains possible owing to the van der Waals component).

The effect of the ionic strength and cationic composition of solution on the conformation of DNA molecules adsorbed on the surface of the stearylamine nanotemplate was explored. For example, an increase in the ionic strength entails the compaction of DNA on the surface (decrease in $\langle R^2 \rangle$ for fixed-length DNA segments), while the addition of 10 mM MgCl_2 solution leads to the formation of dense “sheet” DNA structures in which a DNA strand is packed into stearylamine adjacent lamellas (Fig. 4e) [127]. These results are attributed to a decrease in the effective rigidity of a DNA molecule related to the screening of a part of its negative charge and the Debye screening effect which allows DNA segments to approach each other at a width of one stearylamine lamella. It was shown that the scaling exponent ν is independent of the ionic strength in the range of 0–20 mM [127]. The values of ν and effective persistence length P for DNA

Table 1. Scaling exponent ν and effective persistence length P for DNA adsorbed on the modified HOPG surface from various solutions

DNA kind	Modifier	Solution	Medium in AFM	ν	P , nm	References
Double-stranded (λ)	Stearylamine	Water	Air	0.52 ± 0.02 ($l > 200$ nm) 0.87 ± 0.01 ($l \leq 200$ nm)	31 ± 2	124
Double-stranded (linearized plasmid, 2000 base pairs)	Stearylamine	Water	Air	0.53 ± 0.02 ($l > 250$ nm)	34 ± 2	124
Double-stranded (T7)	Stearylamine	20 mM NaCl	20 mM NaCl solution	0.51 ± 0.01	—	125
Double-stranded (T7)	Stearylamine	20 mM NaCl	20 mM NaCl solution	0.51 ± 0.01	—	125
Double-stranded (T7)	Stearylamine	5 mM MgCl ₂	5 mM MgCl ₂ solution	0.54 ± 0.02	—	125
Double-stranded (λ)	Stearyl alcohol	Water	Air	0.66 ± 0.02 ($l > 400$ nm) 0.87 ± 0.01 ($l \leq 400$ nm)	—	124
Double-stranded (λ)	Stearic acid	Water a	Air	0.93 ± 0.01	—	124
Double-stranded (T7)	Stearic acid	10 mM NaCl	10 mM NaCl solution	0.77 ± 0.01	—	125
Double-stranded (plasmid, 3845 base pairs)	GM	Water	Air	0.59 ± 0.01	—	130
Single-stranded (5386 base pairs)	GM	Water	Air	0.73 ± 0.01	9.1 ± 0.3	134
Single-stranded (5386 base pairs)	GM	~1 mM NaCl	Air	—	6.7 ± 0.2	134
Single-stranded (5386 base pairs)	GM	~10 mM NaCl	Air	—	4.6 ± 0.3	134

adsorbed on the modified HOPG surface from various solutions are listed in Table 1.

Real time in situ AFM studies demonstrated that the thermal motion of DNA molecules on the surfaces of stearylamine and stearic acid nanotemplates has a directed character and the directions of motion coincide with the directions of DNA epitaxy; i.e., DNA segments move along underlying nanotemplate lamellas aligned along three symmetry directions of the HOPG surface (Fig. 6a) [127, 132]. In this case, the movement of DNA segments across lamellas and their out-of-plane movement are also observed.

Study of transcription. Using stearylamine nanotemplate-modified HOPG surface as a substrate, the authors of [132] developed an approach for real time AFM studies of transcription on the scale of single DNA molecules (Fig. 6b). Stopped elongation transcription complexes were adsorbed on the nanotemplate surface, and then during the looped AFM scanning, a set of nucleoside triphosphates was added to solution in which scanning was performed. On the AFM images, the dissociation of RNA polymerase with DNA was observed when transcription was complete. The HOPG surface modified with molecular nanotemplates makes it possible to avoid high ionic

concentrations near the surface which are typical of mica and probably can be applied for the real time AFM probing of other DNA-protein interactions.

Modification with N,N' -(Decane-1,10-diyl)-bis(tetraglycinamide)

For AFM imaging on the modified HOPG surface, a procedure was developed using an oligoglycine-hydrocarbon molecule: N,N' -(decane-1,10-diyl)-bis(tetraglycinamide) ([Gly₄-NHCH₂]₂C₈H₁₆[CH₂NH-Gly₄], **GM**). This linear molecule contains two positively charged (at neutral pH) terminal tetraglycine regions and one hydrophobic central hydrocarbon region with a length of 10 carbon atoms. As opposed to the modifiers described above, GM molecules are well soluble in water and are deposited from aqueous solution by drop casting to form a monolayer with a height of about 0.4 nm [133].

DNA. DNA molecules are adsorbed on the GM-HOPG surface from water or solutions with a weak ionic strength in the unfolded state and enable one to obtain stable AFM images both in an aqueous medium and after drying (Fig. 7) [132, 134, 135]. The morphometric characteristics of DNA on this surface differ

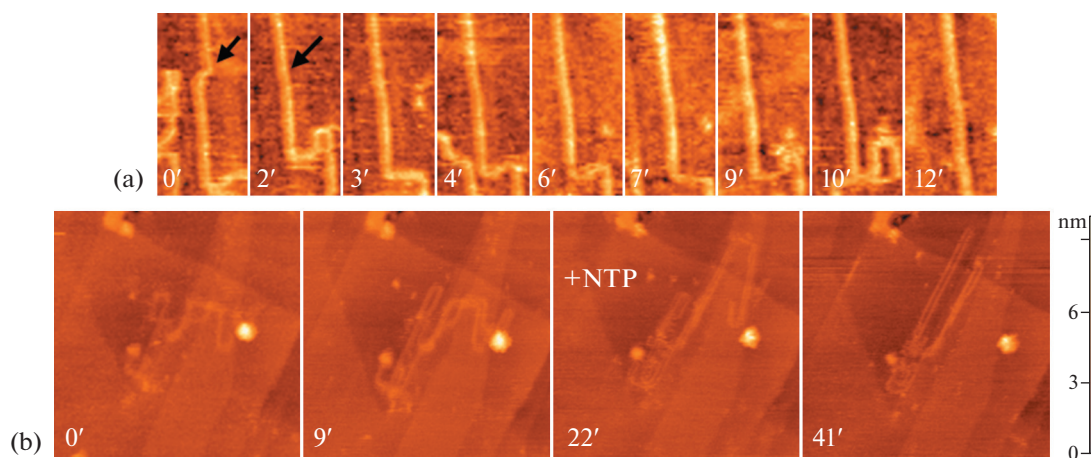


Fig. 6. (a) Sequence of AFM images of the fragment of a T7 bacteriophage DNA molecule adsorbed on the stearylamine self-assembled layer surface on the HOPG surface in 5 mM NaCl solution. The time (in min) of obtaining each AFM image relative to the first one is at the bottom. Arrows show the “hopping” of DNA contour between stearylamine adjacent lamellas. The size of AFM images is $130 \times 220 \text{ nm}^2$ (images are obtained in the tapping mode in the phase channel in solution). Reproduced from [127] under license CC BY-NC 3.0; published by the Royal Society of Chemistry. (b) Sequence of AFM images of stopped elongation complexes on the stearylamine self-assembled layer on the HOPG surface before (frames 1–2) and after (frames 3–4) addition of nucleoside triphosphates. The arrow indicates the RNA polymerase molecules. The time (in min) of obtaining each AFM images relative to the first one is at the bottom. The sizes of AFM images are $500 \times 500 \text{ nm}^2$ (images are taken in the Peak-Force mode in solution). Reprinted with permission from [132]. Copyright (2017) American Chemical Society.

from those on mica. For example, single-stranded DNA is adsorbed on the GM-HOPG surface without secondary structure elements which appear during adsorption on the mica surface (Figs. 7a, 7b) [134, 136]. The height of a molecule calculated from AFM images is somewhat higher for GM-HOPG ($0.35 \pm 0.05 \text{ nm}$ for single-stranded DNA and $0.9 \pm 0.1 \text{ nm}$ for double-stranded DNA) than that for mica (0.3 ± 0.1 and $0.7 \pm 0.1 \text{ nm}$), while the contour lengths of molecules correspond to each other [134]. The uniform adsorption of DNA molecules also proceeds on the GM-modified graphene surface [137].

The adsorption of DNA on the GM-HOPG surface from aqueous solution proceeds owing to electrostatic interaction between amino groups of the GM monolayer and phosphate groups of DNA molecules [134]. The conformation of adsorbed double-stranded DNA molecules is close to the projection of three-dimensional conformation on a two-dimensional surface in the presence of self-crossings ($\nu = 0.59 \pm 0.01$), which corresponds to the kinetic trapping scenario [132, 138]. Actually, using time-lapse real time AFM experiments in water, it was shown that the conformation of DNA on the GM-HOPG surface is fixed; however, an increase in the concentration of NaCl leads to the screening of charges and drives the thermal motion of biomolecules on the surface (Fig. 7d) [132]. It was found that, for the single-stranded DNA on the GM-HOPG surface, $\nu = 0.73 \pm 0.01$, which characterizes its conformation as a self-avoiding random walk [136]. Here, the effective persistence length of the single-

stranded DNA adsorbed on the GM-HOPG surface varies from $\sim 9 \text{ nm}$ for adsorption from solution of a very low ionic strength to $\sim 4.5 \text{ nm}$ for adsorption from 10 mM NaCl solution (Table 1) [136].

The use of the GM-HOPG surface as an AFM substrate made it possible to improve the quality of the morphological analysis of oligonucleotides and nanostructures on their basis. An analysis of AFM images of these structures allowed one to distinguish small changes in the length of oligonucleotides induced by the formation of noncanonical structures [139] and to differentiate between various noncanonical structures with different height [140] and morphology [141, 142].

High-resolution AFM detected an abnormally large amount of kinks of a small radius ($< 3.5 \text{ nm}$) for DNA molecules adsorbed on the GM-HOPG surface upon adsorption from water or solutions with a low ionic strength [138]. These kinks are associated with the local disruption of the integrity of the DNA double helix [143] and the appearance of DNA melting eyes and hairpins inducing the mechanical instability of a biopolymer molecule. Emergence of the DNA undulation was attributed to overcritical bending stress arising owing to the anisotropic electrostatic interaction of DNA with alternating linear rows of positive charges of amino groups on underlying GM lamellas. The described effect emphasizes that one-dimensional periodically charged structures play a special role in interaction with DNA.

Proteins. The conformation and kinetics of adsorption of proteins on the GM-modified HOPG surface differ appreciably from those on unmodified graphite

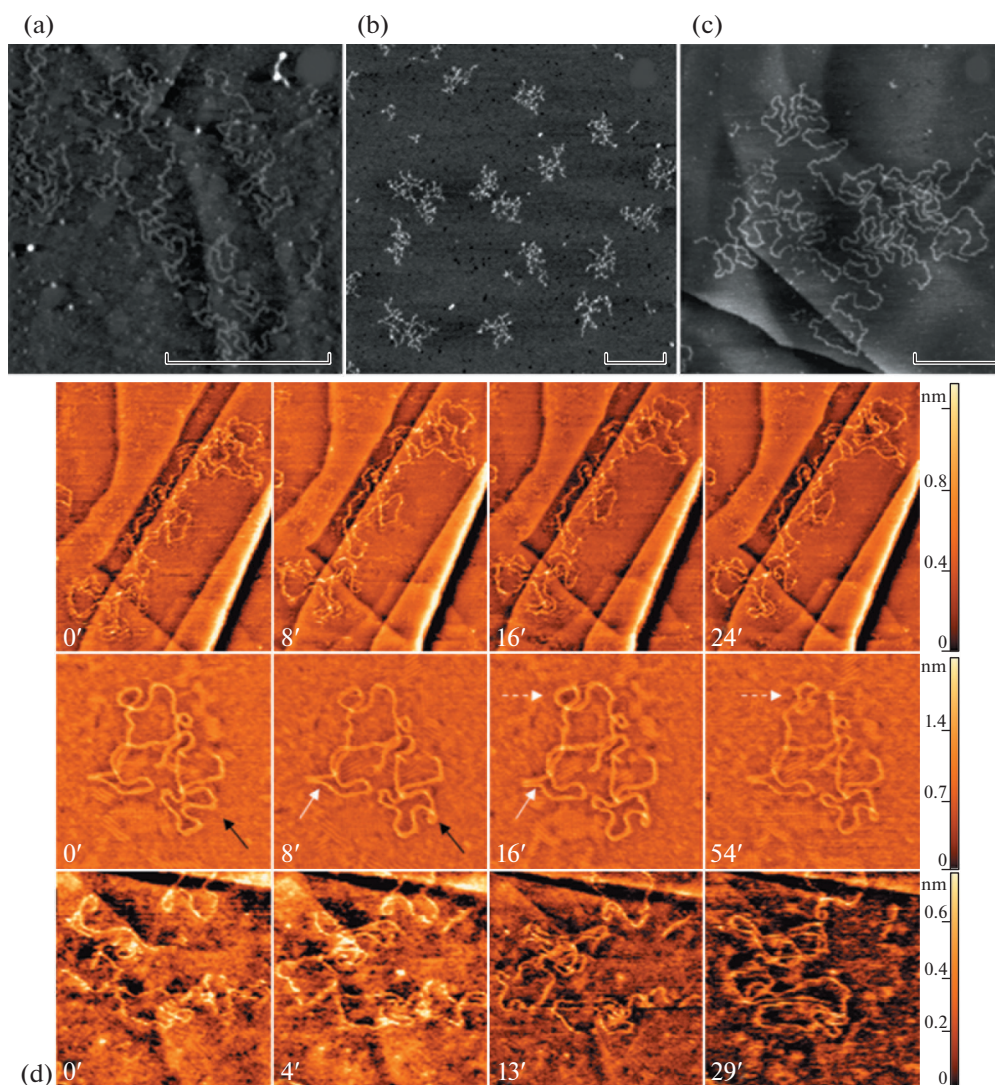


Fig. 7. (a–c) AFM images of (a, b) single-stranded DNA M13mp18 and (c) double-stranded λ -DNA adsorbed from 1 mM tris-HCl buffer on the surface of (a, c) GM-HOPG and (b) mica in the presence of 5 mM Mg^{2+} . Reprinted with permission from [134]. Copyright (2006) the Federation of European Biochemical Societies. (d) Sequences of AFM images of plasmid DNA molecules adsorbed on the GM-HOPG surface from water (the upper row), 5 mM NaCl solution (the middle row), and 100 mM NaCl solution (the lower row). Arrows indicate the motion of segments of DNA molecules. The time of obtaining each AFM image is given relative to the first AFM image of the sequence (in min). The sizes of AFM images are $570 \times 720 \text{ nm}^2$ (upper row), $300 \times 300 \text{ nm}^2$ (middle row), and $500 \times 500 \text{ nm}^2$ (lower row). Reprinted with permission from [132]. Copyright (2017) American Chemical Society. The images are obtained in the tapping mode by the height channel in (a–c) air and (d) solution.

surfaces. The morphological features of proteins deposited on the GM-HOPG surface from 1–50 $\mu\text{g/mL}$ solution in water or physiological buffer at an exposure time after deposition from several seconds to 1 min were studied in air using AFM [74, 79, 133, 144–149]. Some examples are presented in Fig. 8 (the crystallographic structures of the tested proteins visualized using the program NGL Viewer [150] are presented at the bottom).

Under these conditions, fibrinogen is adsorbed on the GM-HOPG surface in the form of single elongated molecules with a well-defined trinodular struc-

ture (Fig. 8a) [74, 79, 133, 144–146]. For external globules, the height is $\sim 3 \text{ nm}$, and for the central globule, the height is $\sim 2 \text{ nm}$ (Fig. 8a). These sizes are much closer to crystallographic sizes (5 and 3 nm, respectively [151]) than the values obtained by AFM on other surfaces, for example, the surfaces of glass and freshly cleaved and modified mica [133, 145]. Moreover, on the GM-HOPG surface, the visualization of additional structural features of a molecule, such as α -C domains, loops of helical regions, and substructure of external globules (γ - and β -knots), becomes possible [133, 144]. Thus, the use of GM-

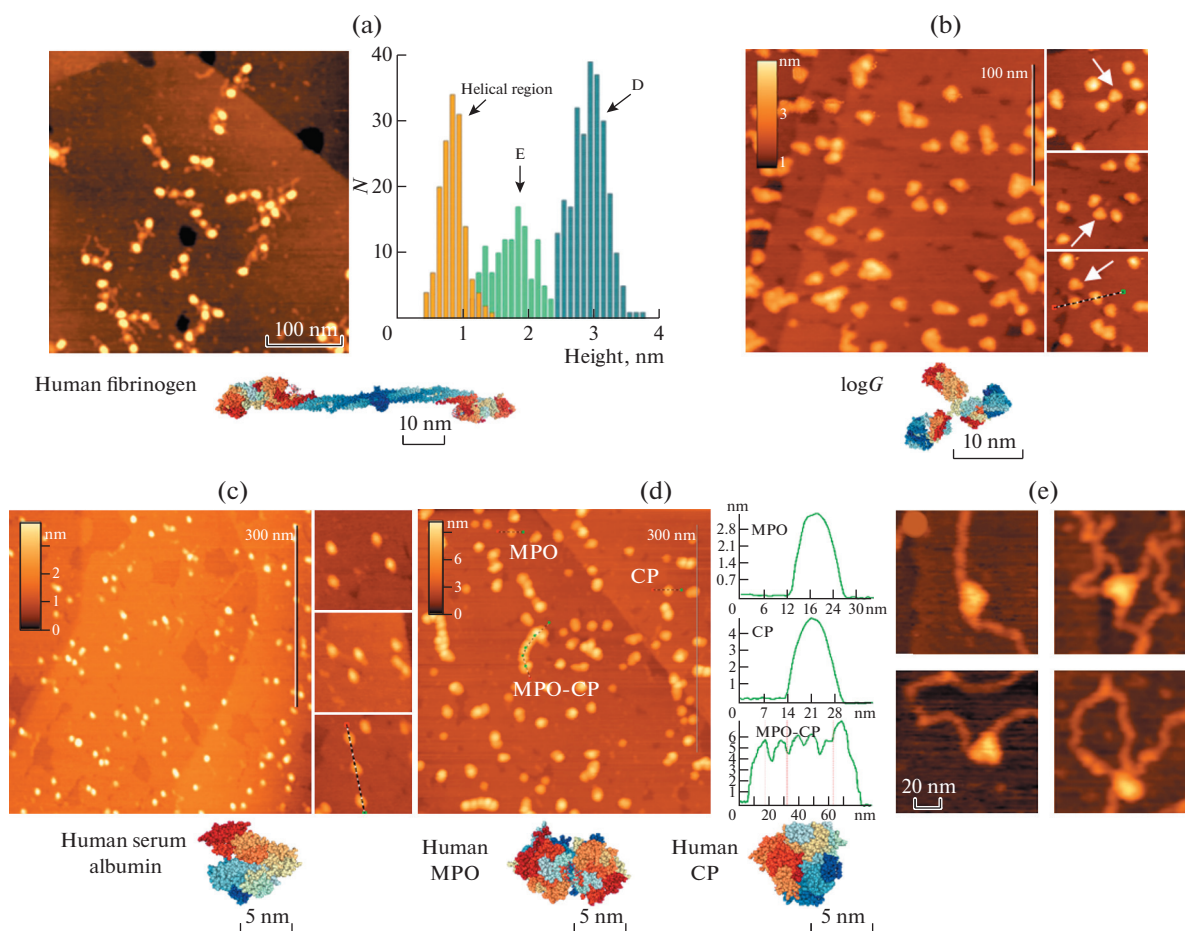


Fig. 8. (a) AFM analysis of proteins and DNA-protein complexes on the GM-HOPG surface. The AFM image of fibrinogen molecules is on the left, and the corresponding height distribution of molecule regions is on the right. Reprinted with permission from [144]. Copyright (2015) the International Society on Thrombosis and Haemostasis; published by Wiley and Sons. The crystal structure of fibrinogen (no. PDB 3GHG) is at the bottom. (b, c) AFM images of (b) IgG (arrows show well-defined Y-shaped molecules) and (c) human serum albumin molecules. Reprinted from [79]. Copyright (2016) with permission from Elsevier. The crystal structures of IgG (no. PDB 1IGT) and human serum albumin (no. PDB 1AO6) are at the bottom. (d) AFM image of single complexes and supercomplexes of myeloperoxidase (MPO) and ceruloplasmin (CP). Profiles of the cross section of the myeloperoxidase, ceruloplasmin, and supercomplex myeloperoxidase-ceruloplasmin molecule are shown on the right along dotted lines on the AFM image. Reprinted from [147]. Copyright (2018) with permission from Elsevier. The crystal structures of human myeloperoxidase (no. PDB 1MHL) and human ceruloplasmin (no. PDB 1KCW) are at the bottom. (e) AFM image of the IgG anti-DNA-DNA complex. Reprinted from [133]. Copyright (2020) with permission from Elsevier. The presented images are obtained in the tapping mode in the height channel in air. The crystal structures of proteins are visualized using the NGL Viewer [150].

HOPG provides an opportunity to improve the reliability of the structural analysis of fibrinogen at the submolecular level.

IgG molecules are adsorbed on the GM-HOPG surface mostly separately in the form of particles with a height of 2.9 ± 0.3 nm and a Y-shaped structure (Fig. 8b) reflecting the crystallographic structure of a molecule and indicating the flat orientation of the adsorbed molecule [79, 133]. A comparison of the average sizes of an IgG molecule derived from the AFM images of protein adsorbed on various surfaces suggests the smallest distortion of height on the GM-HOPG surface [133].

Human serum albumin is also adsorbed on the GM-HOPG surface in the form of single molecules (Fig. 8c). Molecules have an elongated globular shape and the average height of globules is 2.2 nm, which is much higher than the average height of a molecule calculated from AFM images on the surface of mica [152] or silicon [153].

According to AFM studies, a number of other proteins, such as ferritin, myeloperoxidase, lactoferrin, ceruloplasmin, factor XIII, and RNA polymerase, are also adsorbed on the GM-HOPG surface in the native-like conformation with sizes close to crystallographic [79, 147–149]. Using AFM analysis, new structural data on these proteins and their complexes

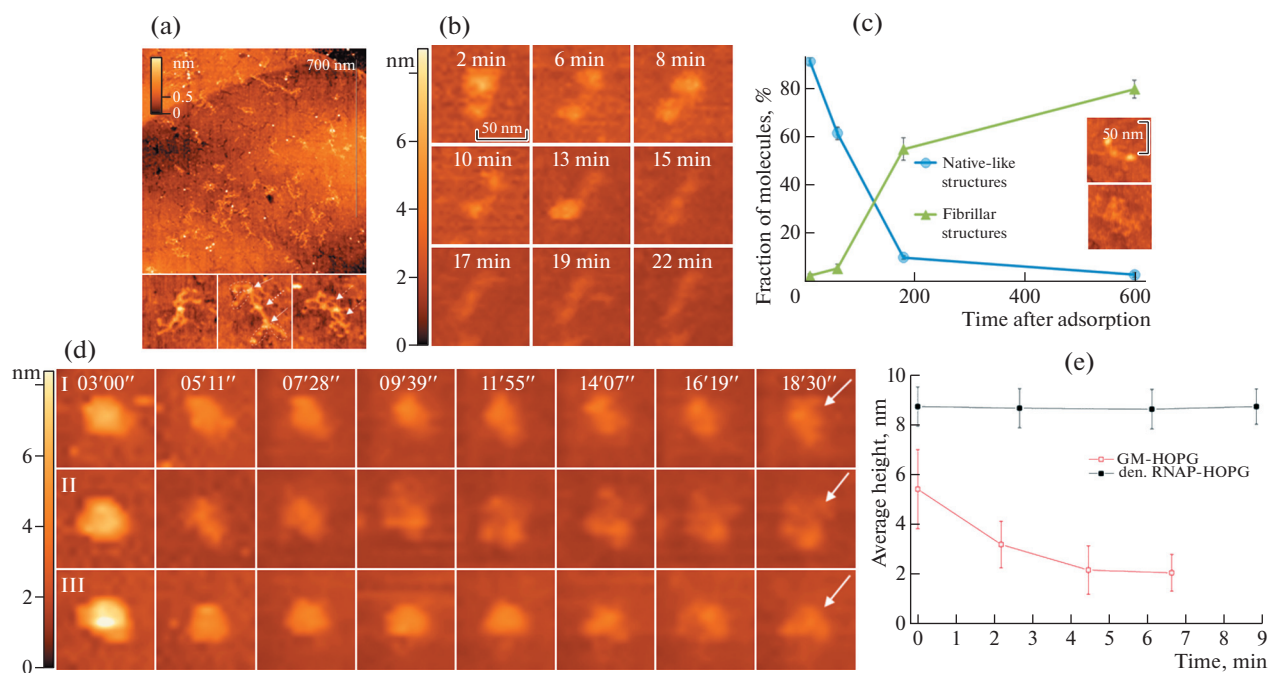


Fig. 9. (a) AFM image ($1 \times 1 \mu\text{m}^2$) of fibrinogen molecules deposited on the GM-HOPG surface and incubated in water for 10 min. The enlarged regions of the surface with unfolded fibrinogen molecules are at the bottom. The point arrow indicates the central region of a molecule, the solid arrows indicate the branching points of fibrills in the outer regions of the molecule, and the dotted arrows indicate fibrills connecting the central region of the molecule to the outer one. Reprinted from [146]. Copyright (2018) with permission from Elsevier. (b) The sequence of AFM images ($100 \times 100 \text{nm}^2$) of the fibrinogen molecule adsorbed on the GM-HOPG surface obtained in the buffer solution. The time of obtaining each AFM image is given relative to the first AFM image of the sequence. (c) Fraction (percentage) of native-like and unfolded fibrinogen molecules as a function of time. (b, c) Reprinted with permission from [74]. Copyright (2019) American Chemical Society. (d) The sequence of AFM images ($100 \times 100 \text{nm}^2$) of *E. coli* RNA polymerase molecules adsorbed on the GM-HOPG surface obtained in water. The time of each AFM image is given relative to the first AFM image of the sequence. Reprinted from [149]. Copyright (2020) with permission from Elsevier. (e) Dependence of the average height of *E. coli* RNA polymerase molecules adsorbed on the HOPG surface modified with GM and denatured protein layer. Reprinted from [149]. Copyright (2020) with permission from Elsevier. The images are obtained in (a, c) the tapping mode in air and (b, d) the PeakForce mode in solution.

were acquired. For example, the nanomorphology of individual complexes of myeloperoxidase with ceruloplasmin and lactoferrin with ceruloplasmin was first characterized, the formation of myeloperoxidase supercomplexes with ceruloplasmin having the structure of densely packed linearly aligned beads (Fig. 8d) was detected [147], and changes in the molecular organization of factor XIII induced by its activation were described [148].

Realization of the kinetic trapping scenario during the adsorption of DNA on the GM-HOPG surface as well as the adsorption of single protein molecules in the native-like conformation on this surface during short-term adsorption implies that the GM-HOPG surface shows promise for the AFM study of the structures and properties of DNA-protein complexes at the level of single molecules. The authors of [133] confirmed that the integrity of DNA complexes with IgG anti-DNA antibodies is retained during their noncovalent adsorption on the GM-HOPG surface (Fig. 8e). Using model systems of Dps protein–DNA

individual complexes and quasi-crystals adsorbed on the GM-HOPG surface, the packing of the genetic material in bacterial cells was investigated [154]. Specifically, the AFM analysis ascertained the nonspecific character of Dps binding to DNA, showed the absence of DNA wrapping around a Dps molecule, estimated the length of region ($\sim 6 \text{ nm}$) for the mutual contact of molecules, and made it possible to propose the linear packing of DNA along rows of ordered Dps molecules in a crystal.

Thus, the GM-HOPG surface holds promise for the structural AFM analysis of single molecules of DNA, proteins, and DNA-protein complexes. This approach may be especially important for the AFM imaging of proteins containing unstructured regions whose structure can hardly be deciphered by crystallographic methods. Moreover, GM-HOPG surface is advantageous for utilization in structural AFM analysis of polysaccharides [155].

Unfolding of proteins. It was shown for several proteins that the conformation of adsorbed molecules

strongly depends on the time of their contact with the GM-HOPG surface. For example, AFM imaging in air after sample drying at different time intervals demonstrated that fibrinogen unfolds into thin fibrillar structures (height, 0.3–2.0 nm) for several minutes upon adsorption on the surface (Figs. 9a, 9c); the unfolding of different globular regions of a molecule proceeds independently of each other [74, 146].

In addition, the GM-HOPG surface-induced unfolding of *E. coli* RNA polymerase holoenzyme and SP6 bacteriophage RNA polymerase molecules into fibrillar structures with a height of 1–2 nm was described [149]. The characteristic unfolding time of the molecules was ~ 7 min, and the effective persistence length of the unfolded molecules was 8 and 11 nm for *E. coli* RNA polymerase and SP6 bacteriophage, respectively. The height and contour and persistence length of fibrils resulting from the unfolding of fibrinogen and RNA polymerase molecules provide evidence that primarily the tertiary structure of these proteins experiences unfolding [74, 146, 149].

Owing to a relatively long characteristic time of unfolding of fibrinogen and *E. coli* RNA polymerase molecules on the GM-HOPG surface (7–10 min), the process of unfolding of single molecules was first visualized in situ in the real-time mode. Figure 9b illustrates the unfolding of a fibrinogen molecule, and Fig. 9d demonstrates the unfolding of *E. coli* RNA polymerase molecules from the native form to the fibrillar one [74, 149]. The time dependence of the average height of adsorbed *E. coli* RNA polymerase molecules (Fig. 9e, lower curve) demonstrates a gradual decrease in height related to protein unfolding. The specific behavior of these two proteins makes it possible to propose that the GM-HOPG surface can induce unfolding of the tertiary structure of other proteins.

A substantial change in the behavior of biopolymers during adsorption on the GM-HOPG surface compared with their behavior during adsorption on the freshly cleaved HOPG surface may be explained by a number of factors. Firstly, there is an increase in hydrophilicity of the surface (manifesting itself as a decrease in the average static water contact angle by 12° – 15° [74, 133]). At the same time, the presence of a hydrophobic hydrocarbon region in GM molecules, that forms extended lamellas on a graphite surface [156], creates the conditions for the unfolding of the protein molecule upon contact with it. Hydrophobicity of the surface is a well-known factor inducing the denaturation of globular proteins during adsorption [59, 60, 70, 157, 158]. Secondly, the presence of electrical charge on the GM-HOPG surface can stabilize the adsorption of protein if it contains an oppositely charged region. Finally, as noted above, the modification of graphite with organic molecules hinders the π – π -stacking interaction of the biopolymer with the HOPG surface which causes the denaturation of DNA and the conformational changes of proteins upon

adsorption. To gain more detailed knowledge of the specific features of interaction between the GM-HOPG surface and proteins, it is advisable to invoke molecular dynamics methods.

The dataset on the morphology of DNA and proteins on the GM-HOPG surface allows one to consider this surface a powerful tool for the structural studies of biopolymers and biopolymer complexes which can improve the accuracy of AFM data. At the same time, peculiarities of the interaction of biopolymers with this surface, such as the DNA undulation at a small ionic strength and the unfolding effect of the GM graphite surface on some proteins on a time scale of several minutes, should be taken into account. Furthermore, the controlled modification of graphite surfaces with other organic compounds seems to be promising for the advancement of AFM of biopolymers.

Modification with Denaturated Protein

The ability of some proteins to undergo strong denaturation during adsorption on the bare HOPG surface was used for modification of the graphite surface with the layer of denaturated protein. Morphological changes in the freshly cleaved HOPG surface after addition of *E. coli* RNA polymerase holoenzyme solution were observed using real-time in situ AFM [149]. It was shown that in this system the denaturated protein layer is initially formed on the HOPG surface (Fig. 10a, frames 1–2), and then native-like RNA polymerase molecules are adsorbed on this layer (Fig. 10a, frames 3–16). Note that RNA polymerase molecules adsorbed on the denaturated protein layer remain stable at least for ~ 1.5 h (Fig. 9e, upper curve; Figs. 10a, 10b). In this case, one can speak about the “antimetamorphic” properties of the HOPG surface modified with the denaturated protein, that is, the surface inducing no conformational changes of proteins adsorbed on it [159], as opposed to the “metamorphic” GM-HOPG surface (and the more so the unmodified HOPG surface) inducing the unfolding of RNA polymerase molecules upon adsorption. Since, as was mentioned above, the freshly cleaved HOPG surface can denature many proteins, formation of the denaturated protein layer acting as a graphite surface modifier may be used for tailoring various graphite biomaterials. It is worth noting that “antimetamorphic” surfaces are in great demand in biomedicine and biotechnology, for example, for the development of biocompatible surfaces or enzyme-based biosensor surfaces [62].

CONCLUSIONS

When graphite surfaces are brought in contact with DNA the π – π -stacking interaction plays a major role, while upon contact with proteins, π – π stacking, van der Waals, and hydrophobic interactions are of prime importance. Interaction with the graphite surface

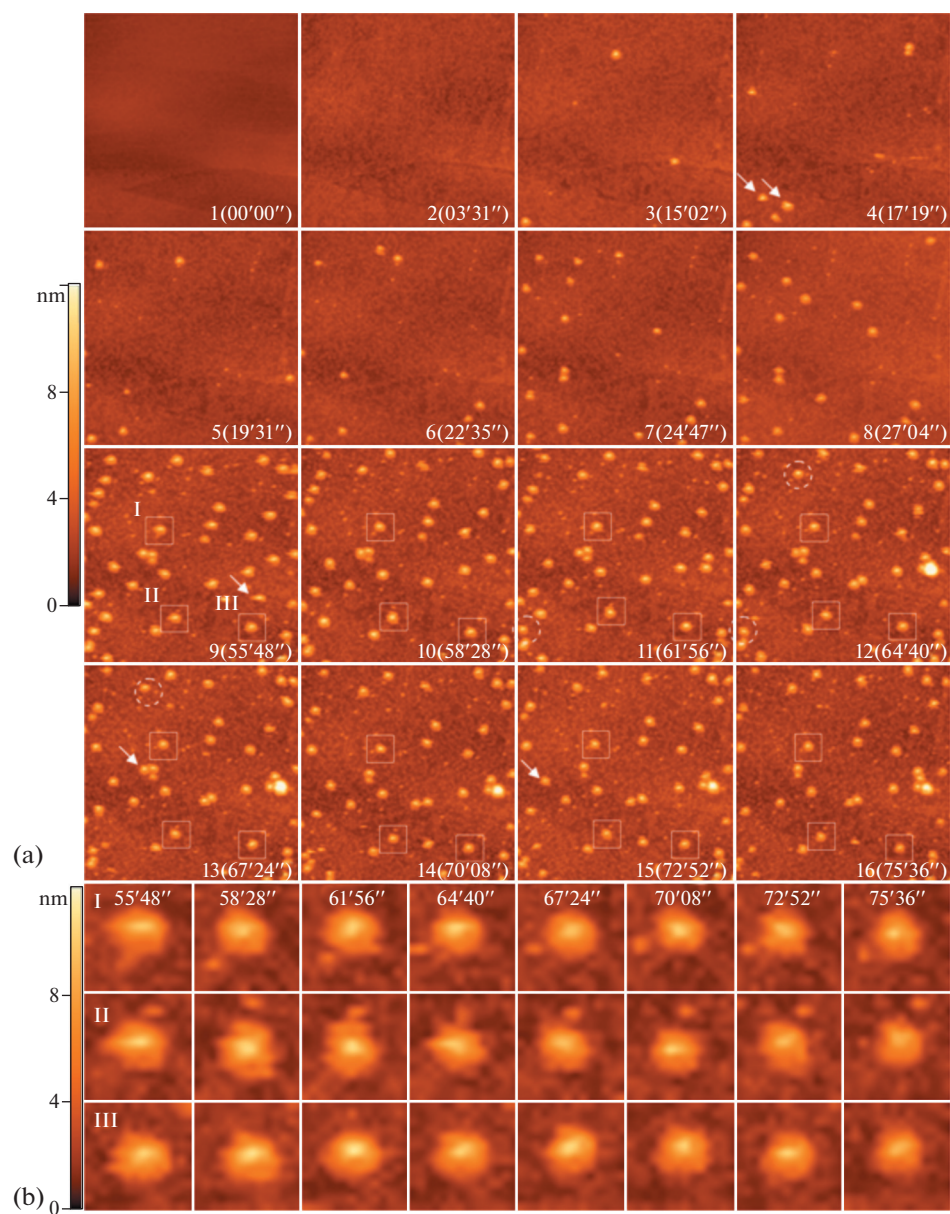


Fig. 10. (a) Sequence of AFM images of the freshly cleaved HOPG surface before (frame 1) and after (frames 2–16) addition of *E. coli* RNA polymerase solution. Numbers and times of obtaining frames are given relative to the first frame. The arrows indicate the examples of deadsorbed molecules, and the dotted circles show regions with the observed surface diffusion of molecules. (b) Series of enlarged images from frames 9–16. AFM images are taken in the PeakForce mode. The sizes of images are (a) $1 \times 1 \mu\text{m}^2$ and (b) $100 \times 100 \text{nm}^2$. Reprinted from [149]. Copyright (2020) with permission from Elsevier. The images are obtained in the PeakForce mode in solution.

induces the dehybridization of DNA molecules, while molecules of many proteins experience denaturation and aggregation on the surface. This limits the use of bare graphite surfaces for the deposition of biopolymers while retaining their native structure. Therefore, application of the freshly cleaved HOPG surface as a substrate for the AFM studies of biopolymers is limited. Moreover, graphite surfaces are strongly liable to random and weakly controlled contaminations from the environment. This worsens reproducibility and

complicates interpretation of the experimental data obtained using this substrate.

Modification of the graphite surface with the (self-assembled) monolayer of organic molecules considerably changes the properties of the surface and the character of its interaction with biopolymer molecules. Depending on the nature of a modifier molecule, DNA molecules adsorbed on the modified HOPG surface can adopt different conformations, including compact globule conformation, self-avoid-

ing random walks, and two-dimensional projection of the three-dimensional coil. This diversity of conformations results from different types and forces of interaction of a biopolymer with the surface. Upon adsorption on modified graphite surfaces, the diameter of DNA molecules and the height of protein molecules are usually less distorted compared with adsorption on the mica surface which is in common use in the AFM analysis of biopolymers.

Using interaction of the GM-HOPG surface with DNA as an example, it is first demonstrated that a periodic linearly distributed charge influences the structure of the adsorbed DNA molecule and leads to appearance of an abnormally large number of small-radius kinks along the contour of a molecule.

The conformation of some proteins on the GM-HOPG surface depends on the time of contact with it. At a fairly short adsorption time (below 1 min), all proteins which have been studied up to now adopt the native-like conformation. Under these deposition conditions, AFM makes it possible to noticeably improve the quality of the structural analysis of some proteins compared with experiments on other substrates and to provide a number of new important observations. As the time of contact of some proteins with the GM-HOPG surface is increased to several minutes, the tertiary structure of protein molecules slowly unfolds and globular structures convert into fibrillar ones.

Using AFM analysis, it is shown that the conformation of RNA polymerase molecules is stabilized upon adsorption on the HOPG surface modified with the layer of the same protein denatured through interaction with the freshly cleaved HOPG surface. This approach to modification of the graphite surface can be utilized for the development of biocompatible surfaces widely demanded in biotechnology.

A wide variety of conformations and kinetics of adsorption of DNA and protein molecules on modified graphite surfaces renders these surfaces promising for wide use in biotechnology and medicine. In addition, modified (specifically, with *N,N'*-(decane-1,10-diyl)-bis(tetraglycinamide)) HOPG surfaces are promising substrates for the development of AFM-based structural analysis of DNA, proteins, and structures on their basis.

FUNDING

This work was supported by the Russian Foundation for Basic Research (project no. 20-13-50047).

REFERENCES

- G. Binnig, C. Quate, and C. Gerber, *Phys. Rev. Lett.* **56**, 930 (1986).
- H. G. Hansma, R. L. Sinsheimer, J. Groppe, T. C. Bruice, V. Elings, G. Gurley, M. Bezanilla, I. A. Mastrangelo, P. V. C. Hough, and P. K. Hansma, *Scanning* **15**, 296 (1993).
- R. Lal and S. A. John, *Am. J. Physiol.: Cell Physiol.* **266**, 1 (1994).
- D. J. Müller, H. Janovjak, T. Lehto, L. Kuerschner, and K. Anderson, *Prog. Biophys. Mol. Biol.* **79**, 1 (2002).
- Y. F. Dufrêne, T. Ando, R. Garcia, D. Alsteens, D. Martinez-Martin, A. Engel, C. Gerber, and D. J. Müller, *Nat. Nanotechnol.* **12**, 295 (2017).
- M. O. Gallyamov, *Macromol. Rapid Commun.* **32**, 1210 (2011).
- U. M. Mirsaidov, H. Zheng, Y. Casana, and P. Matsudaira, *Biophys. J.* **102**, L15 (2012).
- B. Carter and D. B. Williams, *Transmission Electron Microscopy: Diffraction, Imaging and Spectrometry* (Springer, Switzerland, 2016).
- K. D. Jandt, *Adv. Eng. Mater.* **9**, 1035 (2007).
- L.-C. Xu, J. W. Bauer, and C. A. Siedlecki, *Colloids Surf., B* **124**, 49 (2014).
- A. M. Pinto, I. C. Gonçalves, and F. D. Magalhães, *Colloids Surf., B* **111**, 188 (2013).
- Q. Fu, Y. Si, L. Liu, J. Yu, and B. Ding, *J. Colloid Interface Sci.* **555**, 11 (2019).
- Y. L. Lyubchenko and L. S. Shlyakhtenko, *Methods* **47**, 206 (2009).
- Y. L. Lyubchenko, *Biophys. Rev.* **6**, 181 (2014).
- Y. L. Lyubchenko, *J. Phys. D: Appl. Phys.* **51**, 403001 (2018).
- E. C. Beckwitt, M. Kong, and B. Van Houten, *Semin. Cell Dev. Biol.* **73**, 220 (2018).
- M. A. Skabkin, O. I. Kiselyova, K. G. Chernov, A. V. Sorokin, E. V. Dubrovin, I. V. Yaminsky, V. D. Vasiliev, and L. P. Ovchinnikov, *Nucleic Acid Res.* **32**, 5621 (2004).
- D. J. Billingsley, W. A. Bonass, N. Crampton, J. Kirkham, and N. H. Thomson, *Phys. Biol.* **9**, 021001 (2012).
- J. Chao, P. Zhang, Q. Wang, N. Wu, F. Zhang, J. Hu, C. H. Fan, and B. Li, *Nanoscale* **8**, 5842 (2016).
- J. Adamcik and R. Mezzenga, *Macromolecules* **45**, 1137 (2012).
- H. Sanchez, Y. Suzuki, M. Yokokawa, K. Takeyasu, and C. Wyman, *Integr. Biol.* **3**, 1127 (2011).
- Q. Zhong, D. Inniss, K. Kjoller, and V. Elings, *Surf. Sci.* **290**, L688 (1993).
- K. Xu, W. Sun, Y. Shao, F. Wei, X. Zhang, W. Wang, and P. Li, *Nanotechnol. Rev.* **7**, 605 (2018).
- B. Stokke and D. Brant, *Biopolymers* **30**, 1161 (1990).
- F. Valle, M. Favre, P. De Los Rios, A. Rosa, and G. Dietler, *Phys. Rev. Lett.* **95**, 158105 (2005).
- E. Ercolini, F. Valle, J. Adamcik, G. Witz, R. Metzler, P. De Los Rios, J. Roca, and G. Dietler, *Phys. Rev. Lett.* **98**, 058102 (2007).
- C. Rivetti, M. Guthold, and C. Bustamante, *J. Mol. Biol.* **264**, 919 (1996).
- C. Frontali, E. Dore, A. Ferrauto, E. Gratton, A. Bettini, M. Pozzan, and E. Valdevit, *Biopolymers* **18**, 1353 (1979).

29. D. J. Müller, M. Amrein, and A. Engel, *J. Struct. Biol.* **119**, 172 (1997).
30. R. M. Pashley, *J. Colloid Interface Sci.* **80**, 153 (1981).
31. J. Vesenka, M. Guthold, C. Tang, D. Keller, E. Delaine, and C. Bustamante, *Ultramicroscopy* **42**, 1243 (1992).
32. H. K. Christenson and N. H. Thomson, *Surf. Sci. Rep.* **71**, 367 (2006).
33. D. Pastre, O. Pietrement, P. Fusil, F. Landousy, J. Jusset, M. O. David, C. Hamon, E. Le Cam, and A. Zozime, *Biophys. J.* **85**, 2507 (2003).
34. I. Sorel, O. Piétrement, L. Hamon, S. Baconnais, E. Le Cam, and D. Pastré, *Biochemistry* **45**, 14675 (2006).
35. R. L. McCreery, *Chem. Rev.* **108**, 2646 (2008).
36. A. A. Ensafi, E. Heydari-Bafrooei, M. Dinari, and S. Mallakpour, *J. Mater. Chem. B* **2**, 3022 (2014).
37. A. Walcarius, *Trends Anal. Chem.* **38**, 79 (2012).
38. A. Bonanni and M. Pumera, *ACS Nano* **5**, 2356 (2011).
39. S. K. Jang, J. Jang, W.-S. Choe, and S. Lee, *ACS Appl. Mater. Interfaces* **7**, 1250 (2015).
40. A. Vesel, K. Elersic, M. Modic, I. Junkar, and M. Mozetic, *Materials* **7**, 2014 (2014).
41. V. Pesakova, Z. Klezl, K. Balik, and M. Adam, *J. Mater. Sci.: Mater. Med.* **11** (12), 793 (2000).
42. L. Zhang, Y. Sheng, A. Z. Yazdi, K. Sarikhani, F. Wang, Y. Jiang, J. Liu, T. Zheng, W. Wang, P. Ouyang, and P. Chen, *Nanoscale* **11**, 2999 (2019).
43. X.-Q. Wei, L.-Y. Hao, X.-R. Shao, Q. Zhang, X.-Q. Jia, Z.-R. Zhang, Y.-F. Lin, and Q. Peng, *ACS Appl. Mater. Interfaces* **7**, 13367 (2015).
44. M. Zheng, A. Jagota, E. D. Semke, B. A. Diner, R. S. Mclean, S. R. Lustig, R. E. Richardson, and N. G. Tassi, *Nat. Mater.* **2**, 338 (2003).
45. B. S. Husale, S. Sahoo, A. Radenovic, F. Traversi, P. Annibale, and A. Kis, *Langmuir* **26**, 18078 (2010).
46. S. Manohar, A. R. Mantz, K. E. Bancroft, C.-Y. Hui, A. Jagota, and D. V. Vezenov, *Nano Lett.* **8**, 4365 (2008).
47. X. Xiong, J. Han, Y. Chen, S. Li, W. Xiao, and Q. Shi, *Nanotechnology* **32**, 055601 (2020).
48. J. E. Freund, M. Edelwirth, P. Kröbel, and W. M. Heckl, *Phys. Rev. B* **55**, 5394 (1997).
49. M. Edelwirth, J. Freund, S. J. Sowerby, and W. M. Heckl, *Surf. Sci.* **417**, 201 (1998).
50. J. Antony and S. Grimme, *Phys. Chem. Chem. Phys.* **10**, 2722 (2008).
51. S. J. Sowerby, C. A. Cohn, W. M. Heckl, and N. G. Holm, *Proc. Natl. Acad. Sci. U. S. A.* **98**, 820 (2001).
52. X. Shi, Y. Kong, Y. Zhao, and H. Gao, *Acta Mech. Sin.* **21**, 249 (2005).
53. L. Lin, Y. Liu, X. Zhao, and J. Li, *Anal. Chem.* **83**, 8396 (2011).
54. K. B. Ricardo, A. Xu, M. Salim, F. Zhou, and H. Liu, *Langmuir* **33**, 3991 (2017).
55. L. Tang, H. Chang, Y. Liu, and J. Li, *Adv. Funct. Mater.* **22**, 3083 (2012).
56. S. He, B. Song, D. Li, C. Zhu, W. Qi, Y. Wen, L. Wang, S. Song, H. Fang, and C. Fan, *Adv. Funct. Mater.* **20**, 453 (2010).
57. H. S. Kim, N. A. Brown, S. Zauscher, and Y. G. Yingling, *Langmuir* **36**, 931 (2020).
58. D. Coglitore, J.-M. Janot, and S. Balme, *Adv. Colloid Interface Sci.* **270**, 278 (2019).
59. M. Rabe, D. Verdes, and S. Seeger, *Adv. Colloid Interface Sci.* **162**, 87 (2011).
60. W. Norde and J. Lyklema, *Adv. Colloid Interface Sci.* **179**, 5 (2012).
61. Z. J. Deng, M. Liang, M. Monteiro, I. Toth, and R. F. Minchin, *Nat. Nanotechnol.* **6**, 39 (2011).
62. J. M. Bolivar and B. Nidetzky, *Biochim. Biophys. Acta, Proteins Proteomics* **1868**, 140333 (2020).
63. J. Liu and Q. Peng, *Acta Biomater.* **55**, 13 (2017).
64. W. Norde, *Colloids Surf., B* **61**, 1 (2008).
65. W. Norde and C. E. Giacomelli, *J. Biotechnol.* **79**, 259 (2000).
66. E. P. Vieira, S. Rocha, Pereira M. Carmo, H. Möhwald, and M. A. N. Coelho, *Langmuir* **25**, 9879 (2009).
67. A. Sethuraman and G. Belfort, *Biophys. J.* **88**, 1322 (2005).
68. J. S. Sharp, J. A. Forrest, and R. A. L. Jones, *Biochemistry* **41**, 15810 (2002).
69. T. J. Su, J. R. Lu, R. K. Thomas, Z. F. Cui, and J. Penfold, *J. Colloid Interface Sci.* **203**, 419 (1998).
70. D. R. Lu and K. Park, *J. Colloid Interface Sci.* **144**, 271 (1991).
71. M. W. Mosesson, *J. Thromb. Haemostasis* **3**, 1894 (2005).
72. T. C. Ta, M. T. Sykes, and M. T. McDermott, *Langmuir* **14**, 2435 (1998).
73. T. C. Ta and M. T. McDermott, *Colloids Surf., B* **32**, 191 (2003).
74. E. V. Dubrovin, N. A. Barinov, T. E. Schäffer, and D. V. Klinov, *Langmuir* **35**, 9732 (2019).
75. A. Agnihotri and C. A. Siedlecki, *Langmuir* **20**, 8846 (2004).
76. K. L. Marchin and C. L. Berrie, *Langmuir* **19**, 9883 (2003).
77. R. T. T. Gettens, Z. J. Bai, and J. L. Gilbert, *J. Biomed. Mater. Res., Part A* **72**, 246 (2005).
78. R. Ohta, N. Saito, T. Ishizaki, and O. Takai, *Surf. Sci.* **600**, 1674 (2006).
79. N. A. Barinov, V. V. Prokhorov, E. V. Dubrovin, and D. V. Klinov, *Colloids Surf., B* **146**, 777 (2016).
80. G. Vidarsson, G. Dekkers, and T. Rispens, *Front. Immunol.* **5**, 1 (2014).
81. D. Cullen and C. Lowe, *J. Colloid Interface Sci.* **166**, 102 (1994).
82. J. G. Vilhena, A. C. Dumitru, E. T. Herruzo, J. I. Mendieta-Moreno, R. Garcia, P. A. Serena, R. Pérez, *Nanoscale* **8**, 13463 (2016).
83. A. Bujacz, *Acta Crystallogr., Sect. D: Biol. Crystallogr.* **68**, 1278 (2012).

84. S. Rauschenbach, F. L. Stadler, E. Lunedei, N. Malinowski, S. Koltsov, G. Costantini, and K. Kern, *Small* **2**, 540 (2006).
85. A. Orasanu-Gourlay and R. H. Bradley, *Adsorpt. Sci. Technol.* **24**, 117 (2006).
86. X. Peng, H. Fu, R. Liu, L. Zhao, Y. Zu, F. Xu, and Z. Liu, *Scanning* **37**, 158 (2015).
87. S. Boussaad, N. J. Tao, and R. Arechabaleta, *Chem. Phys. Lett.* **280**, 397 (1997).
88. Arzola K. Gonzalez, Orive A. Gonzalez, M. C. Arevalo, L. Vazquez, Creus A. Hernandez, and M. A. Falcon, *Int. J. Electrochem. Sci.* **7**, 1011 (2012).
89. V. V. Korolkov, S. Allen, C. J. Roberts, I. Gozes, and S. J. B. Tendler, *Peptides* **62**, 55 (2014).
90. C. Ge, J. Du, L. Zhao, L. Wang, Y. Liu, D. Li, Y. Yang, R. Zhou, Y. Zhao, Z. Chai, and C. Chen, *Proc. Natl. Acad. Sci. U. S. A.* **108**, 16968 (2011).
91. J. Katoch, S. N. Kim, Z. Kuang, B. L. Farmer, R. R. Naik, S. A. Tatulian, and M. Ishigami, *Nano Lett.* **12**, 2342 (2012).
92. T. Alava, J. A. Mann, C. Théodore, J. J. Benitez, W. R. Dichtel, J. M. Parpia, and H. G. Craighead, *Anal. Chem.* **85**, 2754 (2013).
93. J. A. Mann, T. Alava, H. G. Craighead, and W. R. Dichtel, *Angew. Chem., Int. Ed.* **52**, 3177 (2013).
94. B. Hou and A. D. Radadia, *ACS Biomater. Sci. Eng.* **4**, 675 (2018).
95. X. Zou, S. Wei, J. Jasensky, M. Xiao, Q. Wang, C. L. Brooks, and Z. Chen, *J. Am. Chem. Soc.* **139**, 1928 (2017).
96. J. Guo, X. Yao, L. Ning, Q. Wang, H. Liu, *RSC Adv.* **4**, 9953 (2014).
97. T. R. Walsh and M. R. Knecht, *Bioconjugate Chem.* **30**, 2727 (2019).
98. S. Koehler, F. Schmid, and G. Settanni, *Langmuir* **31**, 13180 (2015).
99. G. Raffaini and F. Ganazzoli, *Langmuir* **19**, 3403 (2003).
100. G. Raffaini and F. Ganazzoli, *J. Biomed. Mater. Res., Part A* **76**, 638 (2006).
101. C. Muecksch and H. M. Urbassek, *Langmuir* **27**, 12938 (2011).
102. C. Muecksch and H. M. Urbassek, *Langmuir* **32**, 9156 (2016).
103. C. Muecksch, C. Roesch, C. Mueller-Renno, C. Ziegler, and H. M. Urbassek, *J. Phys. Chem. C* **119**, 12496 (2015).
104. G. Raffaini and F. Ganazzoli, *Langmuir* **20**, 3371 (2004).
105. D. Martinez-Martin, R. Longuinhos, J. G. Izquierdo, A. Marele, S. S. Alexandre, M. Jaafar, J. M. Gomez-Rodriguez, L. Banares, J. M. Soler, and J. Gomez-Herrero, *Carbon* **61**, 33 (2013).
106. Z. Li, Y. Wang, A. Kozbial, G. Shenoy, F. Zhou, R. McGinley, P. Ireland, B. Morganstein, A. Kunkel, and S. P. Surwade, *Nat. Mater.* **12**, 925 (2013).
107. A. Kozbial, Z. Li, J. Sun, X. Gong, F. Zhou, Y. Wang, H. Xu, H. Liu, and L. Li, *Carbon* **74**, 218 (2014).
108. A. Temiryazev, A. Frolov, and M. Temiryazeva, *Carbon* **143**, 30 (2019).
109. S. Seibert, S. Klassen, A. Latus, R. Bechstein, and A. Kühnle, *Langmuir* **36**, 7789 (2020).
110. D. V. Klinov, E. V. Dubrovin, and I. V. Yaminsky, *AIP Conf. Proc.* **696**, 452 (2003).
111. D. V. Klinov, E. V. Dubrovin, and I. V. Yaminsky, *Phys. Low-Dimens. Struct.* **3–4**, 119 (2003).
112. D. V. Klinov, L. P. Martynkina, V. Yu. Yurchenko, V. V. Demin, S. A. Streltsov, Yu. A. Gerasimov, and Yu. Yu. Vengerov, *Russ. J. Bioorg. Chem.* **29**, 363 (2003).
113. A. J. Groszek, *Proc. R. Soc. London, Ser. A* **314** (1519), 473 (1970).
114. S. Medina, J. J. Benitez, M. A. Castro, C. Cerrillos, C. Millan, and M. D. Alba, *Thin Solid Films* **539**, 194 (2013).
115. F. Silly, *Nanotechnology* **23**, 225603 (2012).
116. T. Yang, S. Berber, J.-F. Liu, G. P. Miller, and D. Tomanek, *J. Chem. Phys.* **128**, 124709 (2008).
117. P. Krukowski, Z. Klusek, W. Olejniczak, R. Klepaczko, M. Puchalski, P. Dabrowski, P. J. Kowalczyk, and K. Gwozdziński, *Appl. Surf. Sci.* **255**, 8769 (2009).
118. V. V. Prokhorov, D. V. Klinov, A. A. Chinarev, A. B. Tuzikov, I. V. Gorokhova, and N. V. Bovin, *Langmuir* **27**, 5879 (2011).
119. T. Hiasa and H. Onishi, *Langmuir* **29**, 5801 (2013).
120. I. De Cat, C. Gobbo, B. Van Averbeke, R. Lazzaroni, S. De Feyter, and J. van Esch, *J. Am. Chem. Soc.* **133**, 20942 (2011).
121. P. N. Dickerson, A. M. Hibberd, N. Oncel, and S. L. Bernasek, *Langmuir* **26**, 18155 (2010).
122. D. Boer, T. Habets, M. J. J. Coenen, M. van der Maas, T. P. J. Peters, M. J. Crossley, T. Khoury, A. E. Rowan, R. J. M. Nolte, S. Speller, and J. A. A. W. Elemans, *Langmuir* **27**, 2644 (2011).
123. C. Arrigoni, G. Schull, D. Bleger, L. Douillard, C. Fiorini-Debuisschert, F. Mathevet, D. Kreher, A.-J. Attias, and F. Charra, *J. Phys. Chem. Lett.* **1**, 190 (2010).
124. E. V. Dubrovin, J. W. Gerritsen, J. Zivkovic, I. V. Yaminsky, and S. Speller, *Colloids Surf., B* **76**, 63 (2010).
125. J. Adamcik, S. Tobenas, G. Di Santo, D. Klinov, and G. Dietler, *Langmuir* **25**, 3159 (2009).
126. E. V. Dubrovin, S. Speller, and I. V. Yaminsky, *Langmuir* **30**, 15423 (2014).
127. E. V. Dubrovin, M. Schachtele, and T. E. Schäffer, *RSC Adv.* **6**, 79584 (2016).
128. A. Podesta, M. Indrieri, D. Brogioli, G. S. Manning, P. Milani, R. Guerra, L. Finzi, and D. Dunlap, *Biophys. J.* **89**, 2558 (2005).
129. T. R. Strick, J. F. Allemand, D. Bensimon, A. Bensimon, and V. Croquette, *Science* **271** (5257), 1835 (1996).
130. T. R. Strick, J. F. Allemand, D. Bensimon, and V. Croquette, *Biophys. J.* **74**, 2016 (1998).
131. S. Cocco and R. Monasson, *Phys. Rev. Lett.* **83**, 5178 (1999).

132. E. V. Dubrovin, M. Schächtele, D. V. Klinov, and T. E. Schäffer, *Langmuir* **33**, 10027 (2017).
133. D. V. Klinov, A. D. Protopopova, D. S. Andrianov, R. I. Litvinov, and J. W. Weisel, *Colloids Surf., B* **196**, 111321 (2020).
134. J. Adamcik, D. V. Klinov, G. Witz, S. K. Sekatskii, and G. Dietler, *FEBS Lett.* **580**, 5671 (2006).
135. D. V. Klinov, T. V. Neretina, V. V. Prokhorov, T. V. Dobrynina, K. G. Aldarov, and V. V. Demin, *Biochemistry (Moscow)* **74**, 1150 (2009).
136. K. Rechendorff, G. Witz, J. Adamcik, and G. Dietler, *J. Chem. Phys.* **131**, 095103 (2009).
137. A. V. Frolov, N. A. Barinov, D. V. Klinov, V. V. Koldov, P. V. Lega, A. P. Orlov, and A. M. Smolovich, *J. Commun. Technol. Electron.* **63**, 1226 (2018).
138. V. V. Prokhorov, N. A. Barinov, K. A. Prusakov, E. V. Dubrovin, M. D. Frank-Kamenetskii, and D. V. Klinov, *Nano-Micro Lett.* **13**, 130 (2021).
139. A. V. Sekridova, A. M. Varizhuk, O. N. Tatarinova, V. V. Severov, N. A. Barinov, I. P. Smirnov, V. N. Lazarev, D. V. Klinov, and G. E. Pozmogova, *Biochemistry (Moscow), Suppl. Ser. B* **11**, 62 (2017).
140. A. M. Varizhuk, A. D. Protopopova, V. B. Tsvetkov, N. A. Barinov, V. V. Podgorsky, M. V. Tankevich, M. A. Vlasenok, V. V. Severov, I. P. Smirnov, E. V. Dubrovin, D. V. Klinov, and G. E. Pozmogova, *Nucleic Acid Res.* **46**, 8978 (2018).
141. A. D. Protopopova, V. B. Tsvetkov, A. M. Varizhuk, N. A. Barinov, V. V. Podgorsky, D. V. Klinov, and G. E. Pozmogova, *Phys. Chem. Chem. Phys.* **20**, 3543 (2018).
142. V. A. Brylev, A. V. Ustinov, V. B. Tsvetkov, N. A. Barinov, I. O. Aparin, K. A. Sapozhnikova, Y. Y. Berlina, E. A. Kokin, D. V. Klinov, T. S. Zatsepin, and V. A. Korshun, *Langmuir* **36**, 15119 (2020).
143. A. Vologodskii and M. D. Frank-Kamenetskii, *Nucleic Acid Res.* **41**, 6785 (2013).
144. A. D. Protopopova, N. A. Barinov, E. G. Zavyalova, A. M. Kopylov, V. I. Sergienko, and D. V. Klinov, *J. Thromb. Haemostasis* **13**, 570 (2015).
145. A. D. Protopopova, R. Litvinov, D. K. Galanakis, C. Nagaswami, N. A. Barinov, A. R. Mukhitov, D. V. Klinov, and J. Weisel, *Nanoscale* **9**, 13707 (2017).
146. N. A. Barinov, A. D. Protopopova, E. V. Dubrovin, and D. V. Klinov, *Colloids Surf., B* **167**, 370 (2018).
147. N. A. Barinov, I. I. Vlasova, A. V. Sokolov, V. A. Kostevich, E. V. Dubrovin, and D. V. Klinov, *Biochim. Biophys. Acta, Gen. Subj.* **1862**, 2862 (2018).
148. A. D. Protopopova, A. Ramirez, D. V. Klinov, R. I. Litvinov, and J. W. Weisel, *J. Thromb. Haemostasis* **17**, 737 (2019).
149. E. V. Dubrovin, D. V. Klinov, and T. E. Schäffer, *Colloids Surf., B* **193**, 111077 (2020).
150. A. S. Rose, A. R. Bradley, Y. Valasatava, J. M. Duarte, A. Prlić, and P. W. Rose, *Bioinformatics* **34**, 3755 (2018).
151. J. M. Kollman, L. Pandi, M. R. Sawaya, M. Riley, and R. F. Doolittle, *Biochemistry* **48**, 3877 (2009).
152. A. Quist, L. Bjorck, C. Reimann, S. Oscarsson, and B. Sundqvist, *Surf. Sci.* **325**, L406 (1995).
153. B. Jachimska, K. Tokarczyk, M. Lapeczynska, A. Pucikul-Malinowska, and S. Zapotoczny, *Colloids Surf., A* **489**, 163 (2016).
154. E. V. Dubrovin, L. A. Dadinova, M. V. Petoukhov, E. Yu. Soshinskaya, A. A. Mozhaev, D. V. Klinov, T. E. Schäffer, E. V. Shtykova, and O. V. Batishchev, *J. Mol. Biol.* **433**, 166930 (2021).
155. R. G. Ovodova, S. V. Popov, O. A. Bushneva, V. V. Golovchenko, A. O. Chizhov, D. V. Klinov, and Yu. S. Ovodov, *Biochemistry (Moscow)* **71**, 538 (2006).
156. N. A. Barinov, A. P. Tolstova, E. A. Bersenev, D. A. Ivanov, E. V. Dubrovin, and D. V. Klinov, *Colloids Surf. B* **206**, 111921 (2021).
157. K. Nakanishi, T. Sakiyama, and K. Imamura, *J. Biosci. Bioeng* **91**, 233 (2001).
158. P. Roach, D. Farrar, and C. C. Perry, *J. Am. Chem. Soc.* **127**, 8168 (2005).
159. C. Blaszykowski, S. Sheikh, and M. Thompson, *Trends Biotechnol.* **32**, 61 (2014).

Translated by T. Soboleva